

AN OBJECT-ORIENTED CLASSIFICATION OF MUIR WOODS USING THE
SYNERGY OF LIDAR AND MULTISPECTRAL DATA

A thesis submitted to the faculty of
San Francisco State University
In partial fulfillment of
The Requirements for
The Degree

Masters of Arts
In
Geography and Human Environmental Science:
Resource Management and Environmental Planning

by

Jose Juan Camarena Jr.

San Francisco, California

August 2013

Copyright by
Jose Juan Camarena Jr.
2013

CERTIFICATION OF APPROVAL

I certify that I have read *An Object-Oriented Classification of Muir Woods using the Synergy of LiDAR and Multispectral Data* by Jose Juan Camarena Jr., and that in my opinion this work meets the criteria for approval a thesis submitted in partial fulfillment of the requirements for the degree: Masters of Arts in Geography and Human Environmental Studies: Resource Management and Environmental Planning at San Francisco State University.

Leonhard Blesius
Assistant Professor

Xiaohang Liu
Associate Professor

Ellen Hines
Professor

AN OBJECT-ORIENTED CLASSIFICATION OF MUIR WOODS USING THE
SYNERGY OF LIDAR AND MULTISPECTRAL DATA

Jose Juan Camarena Jr.
San Francisco, California
2013

An Object Based Image Analysis (OBIA) was employed to classify four tree species in a temperate rainforest utilizing the high-resolution WorldView-2 (WV2) sensor (8 bands + panchromatic) and airborne LiDAR (minimally 2 points per square meter). Classification involved first performing a parametric Maximum Likelihood (ML), Spectral Angle Mapper (SAM), and OBIA classification to the study area. Secondly, for each classified image, a LiDAR-derived Canopy Height Model (CHM) was incorporated thereafter. Kappa and z-statistics were calculated and compared for each classification. It was originally hypothesized that an OBIA will provide the best accuracy, and incorporation of a CHM would further increase classification accuracy for all outputs. A series of statistical tests indicated a lack of strength in utilizing the CHM, except when specifying the Coastal Redwood class at $\geq 50\text{m}$. Kappa results are 59% for the OBIA, 46% for ML, and 24% for SAM. CHM increased kappa accuracy by an average of 4.5%.

I certify that the Abstract is a correct representation of the content of this thesis.

Chair, Thesis Committee

Date

ACKNOWLEDGEMENTS

First and Foremost, I would like to thank Nelly Pino for providing much needed guidance and stewardship in matters of life and love. Without Miss Pino, I would have faltered a long time ago, and my educational dreams would be just that--dreams.

I would also like to thank my mother for provided financial assistance. Although overly excessive family burdens and responsibilities imposed by Mom threatened my educational aspirations at every angle, I am blessed to have her. Although having a perfect mother may not exist, but if it did, I would not trade her for perfection.

I would like to express much gratitude and appreciation to my thesis committee chair and committee for their patience and guidance in completing this arduous research. Appreciation is also expressed to the Geography Department and the Golden Gate LiDAR project for providing access and funding for data utilized.

This thesis is also conducted in honor of fallen voices and dreams in Richmond California, and to past teachers who always believed in me.

TABLE OF CONTENTS

List of Tables.....	vi
List of Figures.....	vii
1. Introduction and Background	1
2. Research Problem.....	9
3. Study Area.....	12
4. Methods.....	16
4.1. WV2 Data and Preprocessing.....	16
4.2. LiDAR Data and Preprocessing.....	22
4.3. Training Data Extraction / Field Work.....	25
4.4. OBIA.....	31
4.5. Maximum Likelihood Classification.....	40
4.6. Spectral Angle Mapper Classification.....	41
4.7. Problems Incorporating LiDAR.....	42
4.8. Accuracy Assessment.....	51
5. Results.....	55
6. Discussion.....	68
7. Conclusion.....	71
8. References.....	75

LIST OF TABLES

Table	Page
1. Scholarly Summary of Conclusive Findings on Multi-Sensor Data Fusion.....	11
2. Trees of Redwood Canyon.....	34
3. Class Separation Distance Matrix generated from the FSO tool.....	40
4. Tamhane's Test using Slope.....	50
5. Tamhane's Test using CHM.....	50
6. Summary of Findings for employed Non-Parametric tests	54
7. MLR classification using aspect, slope, and CHM together.....	56
8. MLR classification using CHM only.....	56
9. MLR classification using slope only.....	57
10. MLR using aspect only.....	57
11. Confusion matrix of FSO-NN.....	66
12. Confusion matrix of ML.....	66
13. Confusion matrix of SAM.....	67
14. Confusion Matrix of FSO-NN with CHM \geq 50.....	73
15. Confusion Matrix of ML with CHM \geq 50.....	73
16. Confusion Matrix of SAM with CHM \geq 50.....	74
17. Summary of Classification Results.....	76
18. Summary of z-statistic results.....	76

LIST OF FIGURES

Figure	Page
1. Worldview-2 sensor comparison of Worldview-1 and Quickbird.....	6
2. Study area.....	17
3. Shaded relief of study area: Redwood Canyon.....	20
4. General flowchart of work performed.....	22
5. The Effect of Tree Heights, Sun Elevation Angle, and Topography on Shadows.....	25
6. CHM Clipped to Study Area.....	29
7. Close-up of Clipped Study Area: Cathedral Grove.....	30
8. Trail Map of Muir Woods and surrounding Redwood Canyon.....	32
9. Training samples (n=147) in the study area.....	35
10. Quartile Ranges of Coastal Band for each tree class.....	41
11. Quartile Ranges of Blue band for each tree class.....	42
12. Quartile Ranges of Green band for each tree class.....	42
13. Quartile Ranges of Yellow band for each tree class.....	43
14. Quartile Ranges of Red band for each tree class.....	43
15. Quartile Ranges of Red - Edge band for each tree class.....	44
16. Quartile Ranges of NIR1 band for each tree class.....	44
17. Quartile Ranges of NIR2 band for each tree class.....	45
18. Mean TOA spectral profile per tree class.....	45

LIST OF FIGURES (CONTINUED)

Figure	Page
19. Independent samples median test.....	53
20. Independent samples Kruskal-Wallis test	53
21. Independent samples Jonckheere-Terpstra test for Ordered Alternatives.....	54
22. Distribution of training samples (n=297).....	62
23. Example of Google Earth's "street - view"	64
24. Figure 24. Classification of FSO-NN.....	67
25. Figure 24. Classification of SAM.....	68
26. Figure 24. Classification of ML.....	68
27. Trial-and-Error analysis as CHM increases from 35m in the FSO-NN classification.....	69
28. Trial-and-Error analysis as CHM increases from 35m in the FSO-NN classification.....	70
29. Trial-and-Error analysis as CHM increases from 35m in the FSO-NN classification.....	70
30. Classification of FSO-NN with CHM \geq 50.....	74
31. Classification of FSO-NN with CHM \geq 50.....	75
32. Classification of FSO-NN with CHM \geq 50.....	75
34. Feature Space of Study Area.....	79

LIST OF APPENDICES

Appendix	Page
1. The Pacific Coast Temperate Rainforest.....	94
2. Map of Muir Woods.....	95
3. Calibration Coefficients of WV2 Image.....	96
4. Tools for Collecting Training Samples.....	97

1. INTRODUCTION AND BACKGROUND

Accurately characterizing tree species distribution and bioparametric metrics is critical for active management of forested ecosystems (Jones *et al.* 2010, Plourde *et al.* 2007). The increase of greenhouse gas emissions over the next century is expected to impact ecological systems, particularly arboreal ones (Allen 2009, Allen *et al.* 2010). In California, it is projected that climate change may increase the severity and frequency of forest fires, change weather patterns, and reduce snowpack levels in the Sierra Nevada (Hayhoe *et al.* 2004).

Of increasing concern for arboreal ecosystem management is the Pacific temperate biome (Appendix 1). Its geographical boundaries stretch from the southern coast of Alaska to the north-central coast of California. This biome has four times more productivity than tropical forests (Davis 2000), but is also one of the most endangered as 13 of 25 million hectares have been destroyed since the arrival of European colonialists (Auwaerter and Sears 2006).

Due to the highly varied mountainous terrain, access to this region can be difficult, and therefore remote sensing is the only viable option as a means of measuring arboreal physical characteristics in a spatially and temporally continuous manner (Hyde *et al.* 2005). Recent advances in remote sensing have allowed for a more proficient analysis of vegetation and forest canopies (Antonarakis 2008, Chen *et al.* 2008, Jones *et al.* 2010, Ke *et al.* 2010, Mundt *et al.* 2006, Pu 2004, Onojeghuo and Blackburn 2011,

Salah *et al.* 2006, Zhang *et al.* 2012). Two of those technologies include the Light Detection and Ranging (LiDAR) airborne sensors, and multi and hyperspectral sensors that allow for monitoring of varied environments at finer spectral scales.

LiDAR data has the potential to distinguish forest composition characteristics accurately in a diversity of forest types (Zhang *et al.* 2012a). Furthermore, airborne LiDAR, coupled with a high level of global positional accuracy and point density, is an attractive dataset for estimating a wide range of forest parameters (Stephens *et al.* 2012). LiDAR has been used for vegetation mapping in urban (Chen *et al.* 2009) and non-urban contexts (Antonarakis *et al.* 2008, Ke *et al.* 2010, Puttonen *et al.* 2010, Voss and Sugumaran 2008), even to map invasive trout in Yellowstone Lake (Shaw *et al.* 2008). LiDAR applications capture accurate three-dimensional information for the retrieval of tree heights, canopy structure, forest biomass, and other parameters that conventional optical sensors are unable to retrieve to a high degree of accuracy. Yet LiDAR is not perfect; Hyde *et al.* (2006) complains that LiDAR is incapable of imaging entire landscapes, limits scanning to near nadir to prevent ranging errors, data has coverage gaps due to pitch and roll, and is expensive.

Hyperspectral high-resolution images also provide the opportunity to differentiate small spectral differences and classify individual tree species better, thereby achieving more accurate classifications. Hyperspectral remotely sensed data have been used in mapping vegetation types across an assorted range of environments, such as estuarine

eel-grass communities (Onojeghuo and Blackburn 2011), marshland vegetation (Rosso *et al.* 2005), urban land-use (Xiao *et al.* 2004), and tropical forests (Clark *et al.* 2005).

A study by Clark *et al.* (2005) used a well calibrated hyperspectral imaging spectrometer called HYDICE to classify 7 tree species in an old growth tropical forests in Costa Rica. The authors analyzed leaf, pixel, and crown-scale spectra using Object Based Image Analysis (OBIA) while comparing the performance of linear discriminant analysis (LDA), spectral angle mapper (SAM), and maximum likelihood (ML) classifiers. The objective was to examine the trade-offs between spectral features, leaf to crown spatial scale of measurement, and classification schemes for the automated classification of individual tropical tree species using their reflectance properties. The overall accuracy at the leaf scale using LDA was 100% with 40 hyperspectral bands and 92% with 30 bands. Different band combinations were also tested, and the ML had a 88% overall accuracy using 60 bands at crown scale. The SAM performed the worst (< 51% overall accuracy) and the authors suggested not using the spectral angle mapper (SAM) and maximum likelihood classifiers for dense arboreal habitats.

Unfortunately, hyperspectral sensors are limited by several factors. Cho *et al.* (2009) argue that the high dimensionality of hyperspectral data restricts the function of parametric classifiers for species mapping due to the demand for a large number of training samples. Quackenbush *et al.* (2000) believe hyperspectral data poses challenges to tree classification because the spectral response of individual trees are influenced by

variation in canopy illumination and topographic effects which ultimately affects accuracy (Ke *et al.* 2010).

Classifications performed using such data can introduce salt-and-pepper noise in the output (Ke *et al.* 2010). Weishampel *et al.* (2000) argue that passive optical sensors are limited in their ability to penetrate the upper canopy layer, and are thus better suited for mapping horizontal structure such as urban environments. However, Onejehuo and Blackburn (2011) believe that such shortcomings can be overcome through compression which reduces data dimensionality, while retaining vital spectral information for classification.

In order to compensate for errors apparent in optical sensors, OBIA provides a more functional way of delineating readily usable objects from optical imagery while also combining image processing and GIS functionalities in order to utilize spectral and contextual information in a holistic way (Blaschke 2010). Using two SPOT-5 satellite images merged with a 1-meter color infrared aerial image, Riggan and Weih (2009) compared an OBIA and a Pixel Based Classification (PBC) in a mixed deciduous and evergreen forest within Arkansas. A supervised classification was performed employing a ML classifier. Utilizing error matrices, the Kappa Coefficient, and a two-tailed t-test, results indicate an overall accuracy of 82% for OBIA and 67% for PBC. The PBC misclassified pixels in the spectrally heterogeneous mixed forest classes, but did well for spectrally homogenous classes such as impervious surfaces and farmland. The OBIA

provided better class distinction for all deciduous and evergreen tree classes. The authors cautioned the use of the ML classifier for classifying intraspecies rich mixed forest.

Kamagata *et al.* (2008) studied and compared both techniques in Central Japan amongst slowly urbanizing agriculture-based areas. Using Ikonos imagery, the researchers determined that the PBC was mired with errors, primarily because it had difficulty differentiating between the highly heterogeneous urban-agricultural landscape and shadows. The OBIA improved the accuracy only marginally. Yet the author's believed that the classification method—minimum-distance—was inappropriate for differentiating between evergreen broad-leaf forests, secondary mixed forests, and broad-leaf forests that were in close proximity from one another. Furthermore, they believed that misclassifications were further hampered by employing an inappropriate scale parameter.

An attractive viable alternative to hyperspectral imagery is the WorldView-2 (WV2) sensor. WV2 was launched by DigitalGlobe in 2009, and is the first commercial satellite to feature a high-resolution 1.8 m spatial resolution (at nadir) with 8 multispectral bands. In contrast to QuickBird (see Figure 1) which has similar bands, WV2 provides four new bands: coastal blue (400-450 nm), yellow (585-625), red-edge (705-745 nm) and a second near-IR band (860-1040 nm). A 0.50 m spatial resolution (at nadir) panchromatic band is also included. The additional WV2 red-edge and NIR bands are important in distinguishing and discriminating vegetation types (DigitalGlobe 2010).

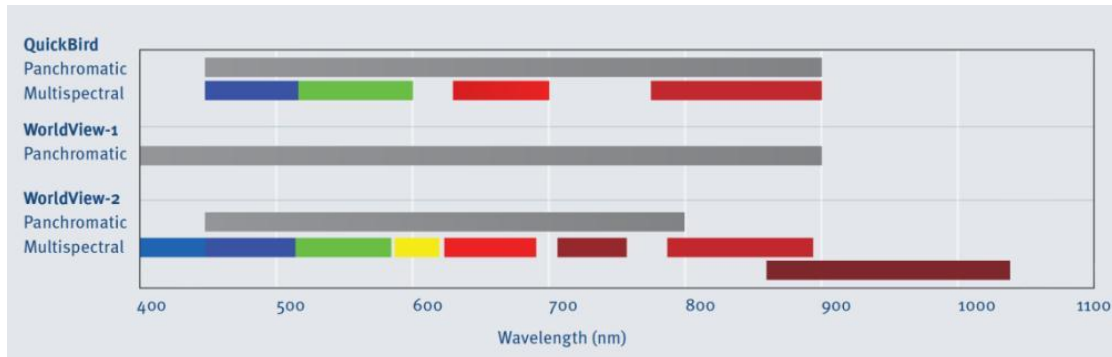


Figure 1. Worldview-2 Sensor Comparison of Worldview-1 and Quickbird (Source: DigitalGlobe 2010).

Studies using WV2 determined that the image texture features extracted from WV2 can be used for modeling and mapping forest structural parameters in conifer plantation forests (Ozdemir and Karnieli (2011)). The WV2 sensors have benefits in urban land use classifications as well; Knovack *et al.* (2011) performed an urban land cover study and determined that classes like ceramic tile roofs and bare soil, as well as asphalt and dark asbestos roofs, can be better distinguished with the additional bands of the WV2 sensor.

Pu and Landry (2012) compared WV2 and IKONOS sensors using a Linear Discriminate Analysis (LDA) and a Regression Tree classification algorithm using OBIA to identify 7 different tree species in a spatially heterogeneous urban environment. Although results indicate that WV2 had an overall average accuracy improvement of 16-18% over IKONOS, WV2 only had an overall average accuracy of 63% and a kappa coefficient of 53%. Cho *et al.* (2009) assessed the spectral configuration of WV2 for

discriminating eight savanna tree species in Kruger National Park of South Africa. The results showed a higher classification accuracy (77%) for the ML classification involving all WV2 bands compared to the traditional blue, green, red and NIR bands (61.8%). The WV2 based classification was improved to 82% (kappa 0.77) when a 3x3 post-classification majority filter was applied.

Other non-arboreal uses for WV2 include a coral reef health study using a Support Vector Machine (SVM) classification that achieved an overall accuracy of 76% using the ocean band alongside the traditional 3 bands, and a 93% accuracy with all 8 bands (Collin and Planes 2012). Chen *et al.* (2009) compared the WV2 and IKONOS imagery for identifying the *Sophora chrysophylla* and *Myoporum sandwicense* tree on the western slope of Mauna Kea, Hawaii using a pixel vs. OBIA approach. WV2, in both the pixel and OBIA approach, had a 6% / 13% improved accuracy over IKONOS.

Since the beginning of the 21st century, an increasing number of studies have attempted to combine multi-source images to improve classification accuracy and overcome challenges posed by using either sensors alone (Chen *et al.* 2009). To date, the synergy or fusion of spectral data and LiDAR has proven successful for a diversity of applications, including the mapping of floodplain vegetation (Geerling *et al.* 2007), reedbed habitats (Onejehuo and Blackburn 2011), urban environments (Chen *et al.* 2009), low (Ke *et al.* 2008) and relatively high (Jones *et al.* 2010) species-rich forests, and deciduous temperate forests (Voss and Sugumaran 2008). These studies indicate an

increase in classification accuracies by 5%-20% when combining LiDAR with an optical sensor.

In a model study by Jones *et al.* (2010) which attempted to classify coastal forests (11 different tree species in total) along Canada's Pacific Coast using fused hyperspectral and LiDAR datasets, results suggest that hyperspectral optical data alone produced an accuracy of over 90% for species within homogenous height, age, and volumetric canopies using a refined Support Vector Machine (SVM) classification. However, the incorporation of height information from LiDAR did not significantly increase accuracy in areas where spectrally similar intra-species tree classes exhibited similar mean canopy heights. The height information from LiDAR resulted in only a slight average per-class accuracy increase of 4%.

Dalponte *et al.* (2008) experimented with different LiDAR returns and channels (elevation and intensity), and different hyperspectral band combinations (25/40/126) using the AISA Eagle hyperspectral sensor for estimating the effectiveness of classifying 19 different tree species in a topographically flat mixed evergreen forest in Italy. Three different classifier were used: (1) distribution-free support vector machines (SVMs), (2) the parametric Gaussian maximum likelihood (ML), and (3) the leave one-out-covariance algorithm (GML-LOOC) classifier. The author's used a Jeffreys–Matusita distance versus the number of hyperspectral channels selected, where saturation was reached at 25 hyperspectral bands. They chose to further analyze the effect on accuracy with 40 and all

126 hyperspectral bands. The use of all 126 hyperspectral bands (versus 25 and 40 bands) and the SVM proved to be the most robust and accurate (88.1% Kappa with 126 bands, 87.9% with 40 bands, and 87.2% with 25 bands) in the exploitation of the multisource data due to its strong non-linear properties and decision boundaries, its ability to manage hyperdimensional feature spaces, and its ability to solve binary classification problems (Dalponte *et al.* (2008). Although the SVM had a higher classification accuracy than the ML (by 10%) or the GML-LOOC (by 20%), the differences in overall and kappa accuracy between the use of all (126) or a fraction (40 or 25) of the hyperspectral bands were insignificant at <1% within each classifier. On average, the inclusion of only the LiDAR first-return height data increased classification accuracy and discrimination of each of the 19 tree species (all of which have very similar spectral signatures but different heights) between 1-10%. Dalponte *et al.* (2008) also concluded that using different LiDAR returns (from 1 to 4) did not increase Kappa significantly.

A summary analysis of the scientific literature within the past 7 years in Table 1 highlights several significant findings, the most obvious being the wide variety of employed classifiers for tree centric classifications. The maximum likelihood (ML) classification appears to be the most widely used. Table 1 also suggests that several studies, including those by Shafri *et al.* (2007) Clark *et al.* (2005) and Pu and Landry (2012), have opted to test and evaluate the performance of two or three classifiers in their

study. Table 1 also suggests that LiDAR will improve classification results between 5% to 20%.

In sum, there is a general consensus from the scientific literature that mapping and discriminating the varied spatial and structural patterns of individual tree species in heterogeneous forests using optical sensors will benefit from the integration of LiDAR datasets (Anderson *et al.* (2008)). Also, as evident in the research discussed, the classifier and the type of environment in which it is used also has a strong impact on accuracy.

Table 1: Scholarly Summary of Conclusive Findings on Multi-Sensor Data Fusion						
Authors	Accuracy Results (%)			Environment Studied	Classifier Used	OBIA? (Y/N)
	Multi / Hyper spectral	LiDAR Only	Both			
Bork and Su (2007)	74.6 (OA)	64.8 (OA)	91 (OA)	Arboreal	Maximum Likelihood (ML)	N
Chen <i>et al.</i> (2009)	69.12 (OA)	n/a	89.4 (OA)	Urban	Hierarchical Tree	Y
Chust <i>et al.</i> (2008) ¹	73.2 / 75.1	n/a	92/88	Coastal	ML	N
Dalponte (2008) ²	88/78/66 (K)	n/a	89/81/71 (K)	Arboreal	SVM / ML / L-NN	N
Geerling <i>et al.</i> (2007)	74 (OA)	78 (OA)	81 (OA)	Mix: grass/bush/forest	ML	N
Jones <i>et al.</i> (2010) ³	72.3 (OA)	n/a	72.9 (OA)	Coastal Forest	SVM	N
Ke <i>et al.</i> (2010) ⁴	88 (K)	87 (K)	92 (K)	Arboreal	Decision Tree	Y
Kempeneers <i>et al.</i> (2009)	55 (OA)	n/a	71 (OA)	Coastal	BLDF	N
Macarau <i>et al.</i> (2011) ⁵	69/63/76 (OA)	32/35/54 (OA)	91/75/87 (OA)	Urban	ML/SVM/INFOFUSE	N
Mundt <i>et al.</i> (2006)	75 (OA)	n/a	89 (OA)	Rangeland Shrub	MTM	N
Onojeghuo and Blackburn (2011)	85 (OA)	n/a	96 (OA)	Coastal Reedbeds	ML	N
Salah <i>et al.</i> (2009) ⁶	50 (OA)	n/a	87 (OA)	Urban	Kohonen's SOM-NN	N
Voss and Sugumaran (2008)	56 (OA)	n/a	75 (OA)	Urban	NN	N
Zhang <i>et al.</i> (2012)	62 (K)	51 (K)	77 (K)	Temperate Rainforest	CART	Y

Note: OA = Overall Accuracy, K = Kappa. Support Vector Machine (SVM), K-Nearest Neighbor (K-NN); where K is a positive integer, Binary Linear Discriminant Function (BLDF), Maximum Likelihood (ML), Kohonen's Self-Organized Map (SOM) Nearest Neighbor (SOM-NN), Classification And Regression Tree (CART). **1.** Mean Producer's Accuracy: Rocky zone / wetland zone **2.** Dalponte tested the accuracy of three classifiers using 24, 40, and 126 hyperspectral bands, but only those with 40 is shown above. "LiDAR only" was also tested, but not described in detail yet it was noted that the accuracy of understory tree's increase 5-15% with only the LiDAR vs. the hyperspectral data. **3.** A Classification using "Three-dimensional canopy volume profiles" were used instead of a traditional pixel-based classification. Although overall accuracy changed minimally between single and fused dataset, producers and user accuracies increased 5-15% depending on the tree species, except for Douglass fir (4.3% producers, -23.2% users) **4.** A Kappa-z test was only provided using discovered optimal scale parameters for each given dataset. **5.** A multilayer perception (MLP) was employed for the data fusion and classification implemented into an Interactive Data Language (IDL). A feed-forward neural network based on a scaled conjugate gradient training was also employed. The classification results shown above are based on accuracy comparisons of using either ML, SVM, INFOFUSE results using the multispectral bands and/or DSM. **6.** Salah *et al.* (2009) also integrated textural features with LARHY which increased overall accuracy by 9%

2. RESEARCH PROBLEM

The synergistic use of LiDAR and WV2 for an OBIA classification of tree species in a highly topographically varied and evergreen temperate rainforest has only been evaluated once in the scientific literature. Zhang *et al.* (2012b) used airborne LiDAR data and WV2 for an OBIA of 4 intraspecies trees using a decision tree (CART) classification in the Strzelecki Ranges, a low mountain range of cool temperate rainforest in southeast Australia. The authors tested the efficiency of CART using LiDAR and WV2 under the following data categories: 1) Utilizing only the blue, green, red, infrared bands (BGR-IR), 2) all WV2 bands, 3) LiDAR and BGR-IR, and 4) LiDAR and all WV2 bands. The authors concluded that the utilization of LiDAR and all WV2 bands had the best accuracy (77% Kappa).

This study aims to fill a gap in the literature by examining the multi-sensor OBIA approach in a temperate rainforest of Northwestern United States. The main objective is to conduct a tree-centric OBIA of Muir Woods and neighboring areas that incorporates part of Tamalpais State Park. Specifically, this research will try to answer two questions: (1) In a topographically heterogeneous and multi-layered temperate rainforest environment of Northwestern California, how significantly different are the classification results of the OBIA from the ML and Spectral Angle Mapper (SAM) classifications? As is evident from the studies previously discussed, it is hypothesized that the OBIA will outperform the pixel-based ML and SAM classifications,

This study also hypothesizes that, based on the scientific literature, the inclusion of LiDAR data will increase classification accuracy by at least 5%. Thus, this research also asks: **(2)** How well does the inclusion of LiDAR data improve the classification accuracy of each classifier. This study hypothesized that, based on the scientific literature as shown in Table 1, the inclusion of LiDAR data will increase classification results by at least 5%.

The ML classifier was chosen for comparison based on its abundant use in the scientific literature. The SAM classifier was chosen as a third classifier based on its utilization in a variety of forest ecosystems, albeit with mixed results (Clark et al. (2005), Petropoulos *et al.* (2010), Shafri *et al.* (2007)).

OBIA was chosen as a main feature of this study because studies have suggested that OBIA generates a much higher accuracy than a pixel-based classification (PBC) and is less susceptible to error. A study by Robertson and King (2011) on the land cover decadal change detection of eastern Ontario determined that, after applying a McNemar's Test for statistical comparisons of both methods, OBIA had fewer significant classified errors than PBC where large entities such as forest stands, wetlands, fields, or urban areas were incorrectly classified.

3. STUDY AREA

Muir Woods National Monument (MWNM), which is administered by the National Park Service (Figure 2) consists of over 500 acres, and is located 20 km north of San Francisco and one mile west of Mill Valley in Marin County (NPS 2008). Located near the southern tip of the coastal temperate rainforest biome, the area consists of a cool maritime climate with a moderate temperature (5 to 21 °C) (Chapman and Reiss 2003).

Fog is common throughout the year, and precipitation can reach between 700 and 3000mm each year although predominantly during the winter season (October - March). Based on its close proximity to the Pacific Ocean, and its northeastern aspect facing deep concave slopes, moisture from fog moderates the dry summer temperatures while providing, on average, an extra one to two meters in precipitation. Most of the maritime fog that rolls into the region, especially in the deep gorge called Redwood Canyon is trapped by the multi-story canopy of Redwoods and Douglas Firs. (Chapman and Reiss 2003, NPS 2008, NPCA 2011).

The mountains found in MWNW and surrounding area are part of a narrow band of low but steep mountains on the western edge of the North American plate. The region began forming around 150 million years ago by bedrock from ancient sea floor sediments and igneous rock that was heavily folded and uplifted due to lateral slipping along the juncture of the North American and Pacific plates (Auwaerter 2006). Muir Woods i



Figure 2: Study Area (Source: Google Maps)

nestled within Redwood Canyon (Figure 3 and Figure 4), one of the main valleys in the region, transformed by the south-trending course of Redwood Creek that begins north near the peak of Mt. Tamalpais.

Redwood and Fern Creek, as shown in Appendix 2, are the primary drainage of the Redwood Creek Watershed. The watershed is underlain by the Franciscan Complex that consists of deformed beds of sedimentary, metamorphic, and igneous rocks from the

Jurassic and Cretaceous age (McLaughlin *et al.* 2000). Soils in the parks are agriculturally poor gray-brown podzolic (alfisols), and plant / tree debris scatter litter the floor (Kimball and Kondolf 2002, NPS 2008, NPS 2011).

It has been documented that fire benefits the long-term health of coastal redwood forests (NPS 2008). Data suggests that fires of low to mid intensity, with rare high intensity that charred large forests, frequented this region every 20 - 50 years before European colonization (Agee 1993). Fire has many benefits, including the clearing of debris so tree seeds can reach mineral soil. Fire also destroys harmful bacteria and fungi that can damage new tree sprouts, and fire turns debris into ash which enhances soil nutrients for seedlings (NPS 2008). Due to fire's importance in the ecology of these forests, the National Park Service conducts prescribed interval burning as a substitute for natural fires.

Although Coastal redwoods (*Sequoia sempervirens*) and Douglas firs (*Pseudotsuga menziesii*) dominate the landscape, other deciduous trees, grasslands, and chaparral can be found within and outside both parks. The multi-layered canopy structure (i.e. a ground herbaceous layer, understory trees, and a top canopy) of this old-growth and spatially heterogeneous forest sustains an ecosystem that produces specialized species of plants and trees. Plants such as *Oxalis oregana* (Redwood Sorrel) and *Anemone oregana* (Windflower) blankets the ground cover of Muir Woods, including

ferns and wildflowers (for a full list of understory plants, see <http://www.marin.edu/cnps/MuirWoods.html>). The understory canopy consist of the *Umbellularia californica* (California Bay Laurel), *Acer macrophyllum* (Big Leaf Maple), *Lithocarpus densiflorus* (Tan Oak), *Torreya californica* (California Nutmeg), *Alnus rubra* (Red Alder), *Aesculus californica* (California Buckeye), and *Quercus agrifolia* (Coast Live Oak; situated mostly on the western coastal side of Muir Woods). *Sequoia sempervirens* (Coastal Redwoods) and Douglas fir (*Pseudotsuga menziesii*) dominate the upper canopy (NPS 2008).

At the preliminary phases of this research, the boundary of the study area was selected to be Muir Woods only. A preliminary survey was performed by walking through most of the trails within Muir Woods, and those outside it. It was determined that Muir Woods is nestled within Redwood Canyon, and the scope of the vegetative characteristics could be better explained if the study area were to be extended to encompass the entire Redwood Canyon. The multi-layered canopy structure that is characteristic of Muir Woods, although common, does not dominate the region. To capture the variability of tree species that exist within Redwood Canyon, which serves as an ecotone between a chaparral and a temperate rainforest environment, the study area was expanded outside the boundaries of Muir Woods and into surrounding sections of Mt. Tamalpais State Park. The yellow boundary shown in Figure 3, is primarily the Panoramic Highway. The Panoramic Highway serves as the northern, eastern, and

western border of the study area. The Old Mine Trail, Dipsey Trail, and Fire Road serve as the southern border of the study area.

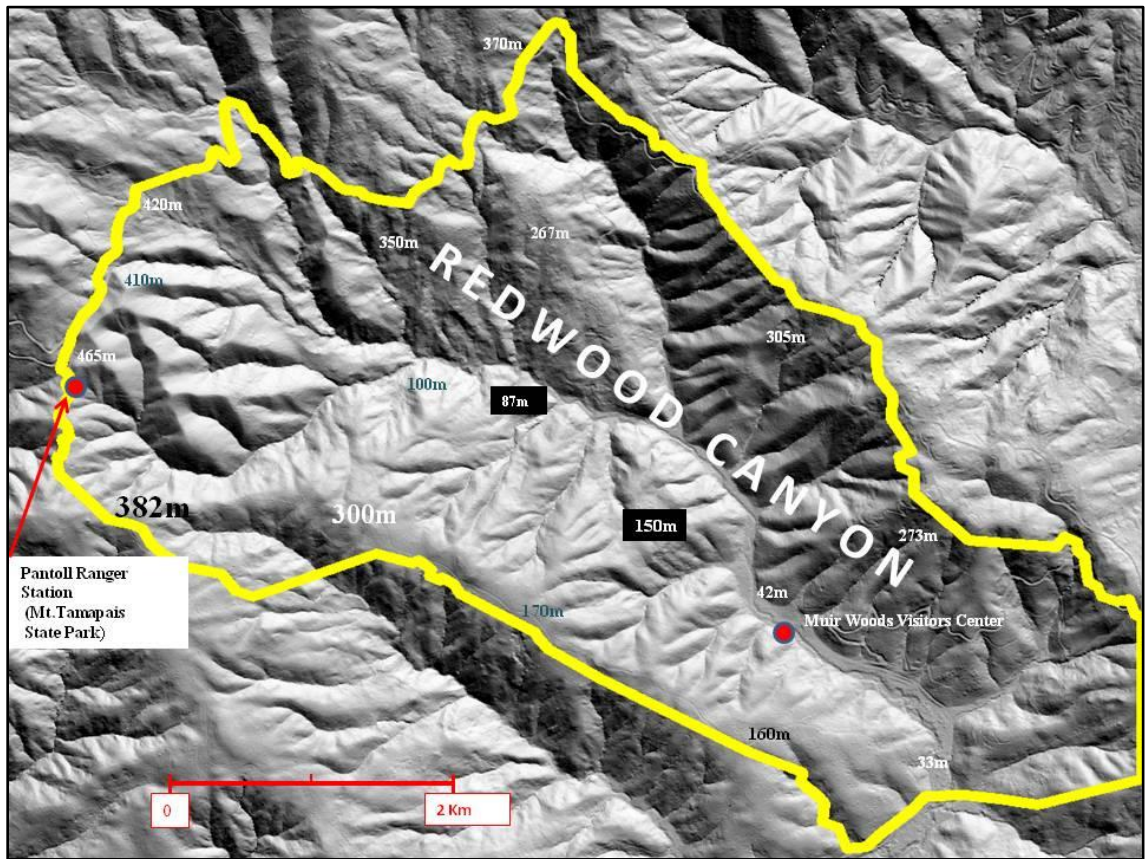


Figure 3. Shaded Relief of Study Area: Redwood Canyo

4. METHODS

4.1 WV2 Data and Preprocessing

The WorldView-2 (WV2) image was acquired on September 1, 2012. Commercially available products of WV2 consist of a 2 m multispectral image with 8 bands and a 0.5 m panchromatic image. The average off nadir angle is 20°. According to the manufacturer, DigitalGlobe, WV2 products are delivered to the customer with radiometrically corrected image pixels (DigitalGlobe n.d.). A relative radiometric correction is performed on raw data from all detectors in all bands in the early stages of WV2 formation. This correction includes a dark offset subtraction and a non-uniformity correction. The image is then spatially resampled to create radiometrically corrected pixels.

Figure 4 provides a flowchart of general procedures conducted in this study. The image was orthorectified using the "Orthorectify Without GCP" tool in Erdas Imagine. The Rational Polynomial Coefficient (RPC) model is an acceptable alternative to physical sensor models method for photogrammetric processing (Chen *et al.* 2006, Fraser *et al.* 2003, Fraser *et al.* 2005, Tong *et al.* 2010). Erdas Imagine 2011 has a RPC geometric model designed for the WV2 image; it is a simpler empirical mathematical

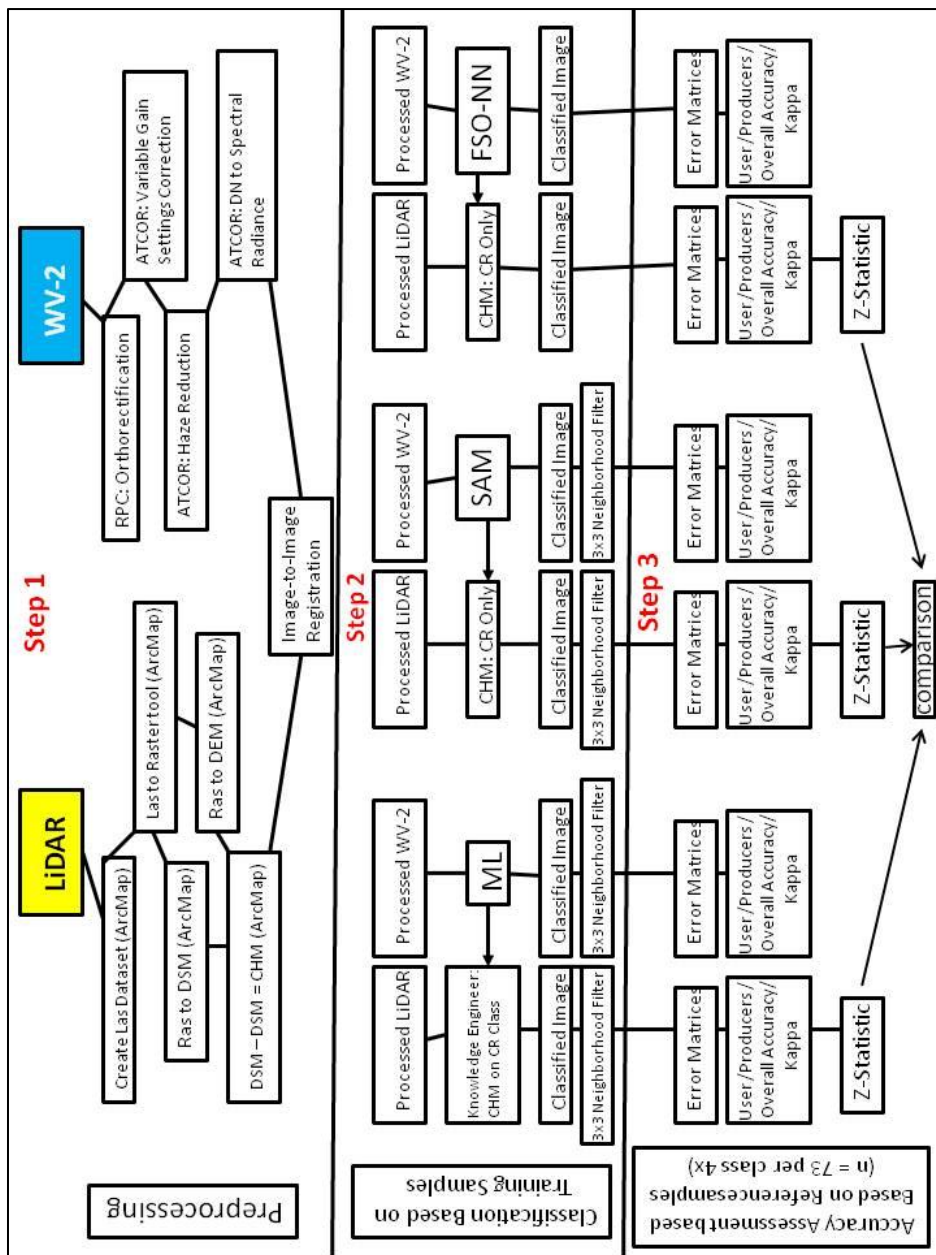


Figure 4. General flowchart of work performed

model relating image space (line and column position) to latitude, longitude, and surface elevation (Zhang *et al.* 2010). The tool requires the input of an RPC located in the metadata file provided by the manufacturer upon purchase. This file contains the information necessary for orthorectification, such as exterior orientation of the satellite when the data was collected (DigitalGlobe n.d.).

The tool also requires the satellite image as input, and a DEM to supply elevation values. The DEM utilized in the RPC tool was created from LiDAR point cloud data. The tool then computes the proper geographic position for each image cell, producing an orthorectified image.

Pan-sharpening was not performed in order to preserve the radiometric integrity of the data. Instead, a haze Reduction and removal was performed next on the WV2 image using ATCOR3, a tool for Atmospheric/Topographic correction of mountainous terrain. ATCOR 3 requires a DEM to obtain information about surface characteristics, such as slope, aspect, shadow, skyview, and sensor information such as zenith and azimuth angles. These datasets are used to derive terrain files for a Haze or Atmospheric correction, along with calculating spectral radiance, ground reflectance, topographic corrections, and extract surface brightness temperatures.

Before the haze removal is performed, the calibration of the WV2 variable gain settings has to be performed. Sensor calibration problems may pertain to spectral

properties; for example, the channel center positions and / or bandwidths might have changed compared to radiometric properties, i.e., the offset (C_0) and slope (C_1) coefficients relating the digital number (DN) to the at-sensor spectral radiance (Richter and Schlapfer 2012).

Unlike hyperspectral imagery, miscalibration is difficult to detect in multispectral imagery, so calibration of the radiometric coefficients is necessary. Calibration is also needed to correctly help ATCOR3 "rescale" the data of the raw DN image to true radiance at sensor, or Top-of-Atmosphere (TOA) radiance, which is then used for the Haze/Atmospheric correction process. TOA spectral radiance is measured in units of $W m^{-2} sr^{-1} nm^{-1}$, where W is watts, m is meter, sr is steradian, and nm is nanometer. The WV2 calibration file provided by ATCOR3 is only a template and must be updated to values found in the metadata file (IMD.). The rescaled calibration file is shown in Appendix 3, and Updike (2010) provides the bandwidths and k factors required by ATCOR3 to transform the raw digital number image into TOA spectral radiance.

Temporal variations in solar illumination and a wide range of topographic landscapes present a problem for classifying trees that have a small sun-lit surface or vegetation covered by tree canopy shadows. The differences in canopy heights and lengths in this region, along with differences in ground elevation create a shading or shadowing effect that induces challenges in classifying neighboring trees (see Figure 5). The atmospheric/topographic correction of ATCOR3 was unable to remove the effect of

tree canopy shadows; topographic correction models (i.e. Minnaert Correction) are limited in their ability to remove the shadowing effect of trees, especially forests of the Pacific Northwest. Unlike smooth terrain, where irradiance and radiance is controlled by the sun-terrain-sensor geometry alone, shadowing by forest canopies is the dominant source of spatial variance (Gu and Gillespie (1988), Kane et al. (2008)). More complex canopies produced lower proportions of sunlit area than less complex canopies for a

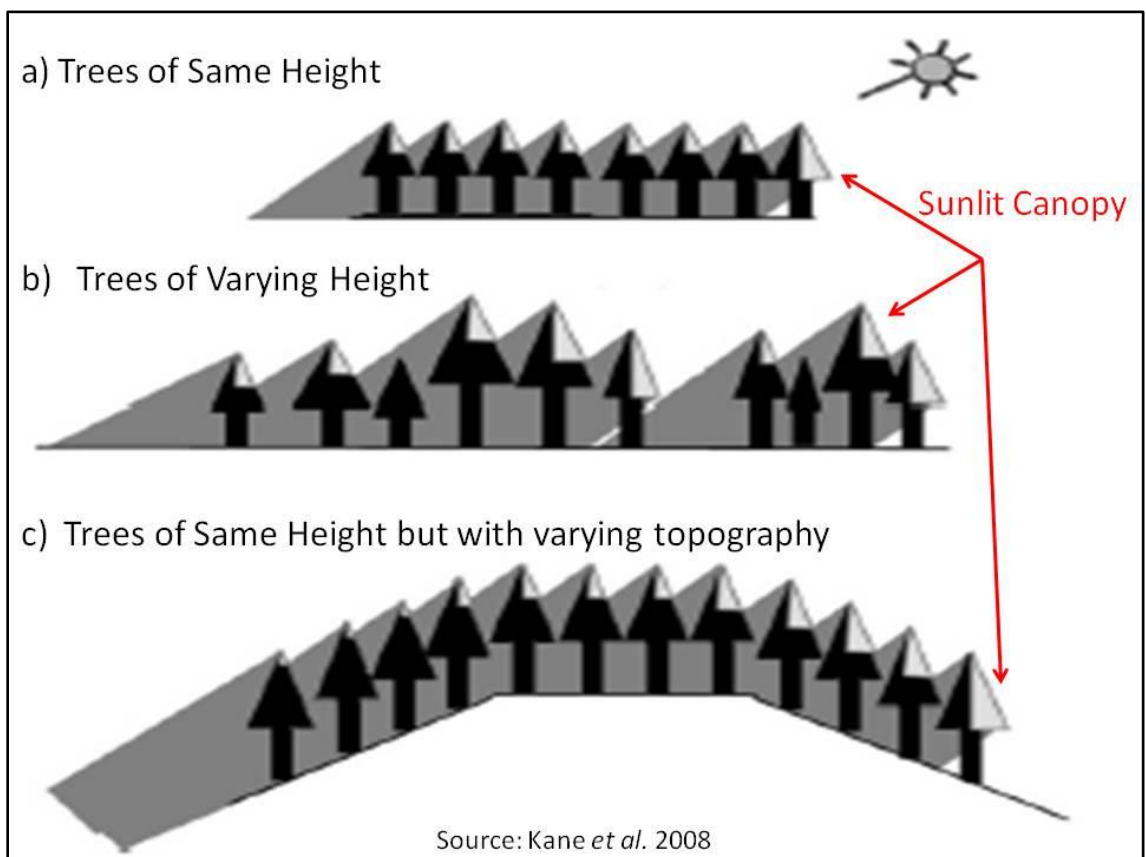


Figure 5. The Effect of Tree Heights, Sun Elevation Angle, and Topography on Shadows. Note: Depending on the Solar Zenith Angle and Incident Angle, the sunlit canopy will vary. This image, taken from Kane et al, (2008), does not show the range of sunlit canopy areas with trees of varying height and varying topography.

given incidence angle (Kane et al 2008). According to Van Pelt and Ndkarmi (2004) and Waring and Franklin (1979), the variations in age, height, and elevation result in a range of canopy structure that is only found in few places on Earth.

Efforts to undertake the removal of tree shadowing was conducted by Kane *et al.* (2008). They conducted a study using LiDAR-derived Canopy Height Models (CHM), and exposed canopy surfaces of 80 conifer stands in the Pacific North-west ranging from pre-canopy closure to old-growth, and adjusted the underlying topography to represent the canopy as it would exist on flat terrain. To accomplish this, the authors tested the performance of the leading topographic correction model called the Sun-Canopy Sensor (SCS) developed by Gu and Gillepsie (1988), a revised version (SCS + C [cosine correction constant]) by Soenen *et al.* (2005), and a newly constructed model called the Adaptive Shade Compensation (ASC) algorithm based on two independent variables. The ASC incorporates the shadow area proportion as an estimator of canopy complexity and the inverse of the SCS $[(\cos\alpha \cos\theta) / \cos i]$; where α is the slope (degrees), θ is the solar zenith angle, and i is the incidence angle (degrees)] as an estimator of how the proportion of shadow area changed based on the geometry of the scene. Results indicated that the robustness of each model depended on the topography and the Solar Zenith Angle (SZA), with the ASC the least effective at steeper slopes and the SCS+C providing substantially more accurate corrections for all SZAs. Yet the authors mention that their results may not

be representative of the performance of the SCS+C correction because they did not fully take into consideration the sky illumination coefficient within the SCS+C algorithm.

The inability to remove the shadow effect caused by the combined effect of canopy structure/ruggedness, the geometry of incidence and exitance angles, and topography can negatively impact classification accuracy (Kane *et al.* 2008). Yet due to the apparent lack of publications devoted to understanding the relationship between tree canopies and shade, and a lack of strong consensus on how to successfully tackle the shade and shadows effect of trees in a topographically complex arboreal environment, this study will not consider appropriately classifying shaded areas that are known to be vegetated. Instead, a simple "shade" class was developed in the mapping of Redwood Canyon.

4.2 LiDAR Data and Preprocessing

The LiDAR data was received from the Golden Gate LiDAR Project, sponsored by the US Geological Survey (USGS) and San Francisco State University. The imagery was collected in 2010 at a nominal point spacing of 2 points per meters for San Mateo, San Francisco, and Marin Counties. The aerial LiDAR sensor was capable of capturing the first, second, third, and last return from a single laser pulse. The first return generated the most data, with 87.98% of all the returns, and the second with 10.34%.

ArcMap 10.1 was used to process the LiDAR point cloud data. The "Las to Raster" tool converted the point cloud into a raster. The tool uses a process called binning

to determine the value of a pixel. Binning examines the points that fall within the pixel, then determines which z-value to use when generating the raster surface if there is more than one point to consider (ESRI 2010).

The "Las to Raster" tool has a section wherein the user can specify the cell size of the new raster. A reasonable cell size of the las raster is four times the average point spacing (APS) according to ArcGIS Help 10.1. If this process is not considered, a lot of noise will manifest in the DEM/DSM because the point cloud is not evenly spaced (ESRI 2012). The Las files in this research has an APS of 0.54m. Multiplying the APS by 4 generates a 2.16 meter cell size. The figure was rounded to 2m in order to match the WV2 image cell size.

The next step was to generate the Digital Surface Model (DSM) and the Digital Elevation Model (DEM). These two datasets are needed to calculate the canopy height model (CHM). Within the "Las to Raster" tool, the DSM is generated by assigning the largest or maximum z-value in the cell while specifying the first pulse return of the point cloud. The DEM is generated by assigning average values of all the z-values within the cell, while specifying the last pulse return. The optional natural neighbor interpolation method in the "Las to Raster" tool was used to define values for cells that do not have points within their extent (i.e. to fill-in voids that have no data).

Once the DSM and DEM datasets are generated, the "raster calculator" in ArcGIS was used to subtract the DSM from the DEM. The output had negative values in very

small areas, so the conditional or "Con" tool was used to provide values at or above zero meters. The CHM, shown in Figure 6 and 7, was then clipped to the study area. Brighter areas indicate higher canopy height elevations, with the tallest tree being located in Muir Woods measured at 73.24 m. The CHM continued to exhibit no-data cells throughout the dataset, therefore gaps were interpolated using a Natural Neighbors algorithm.

The next step was to register the WV2 image and the CHM. Both images have similar cell size. They must be positioned in respect each other so that corresponding elements of the same ground area appear identical in both images. In this study, 75 GCPs selected primarily on road and paved trail intersections were used to complete image-to-image registration. By using the WV2 image as a reference, and the Image Equalizer tool in Erdas Imagine 2011, a 0.46 RMSE was achieved.

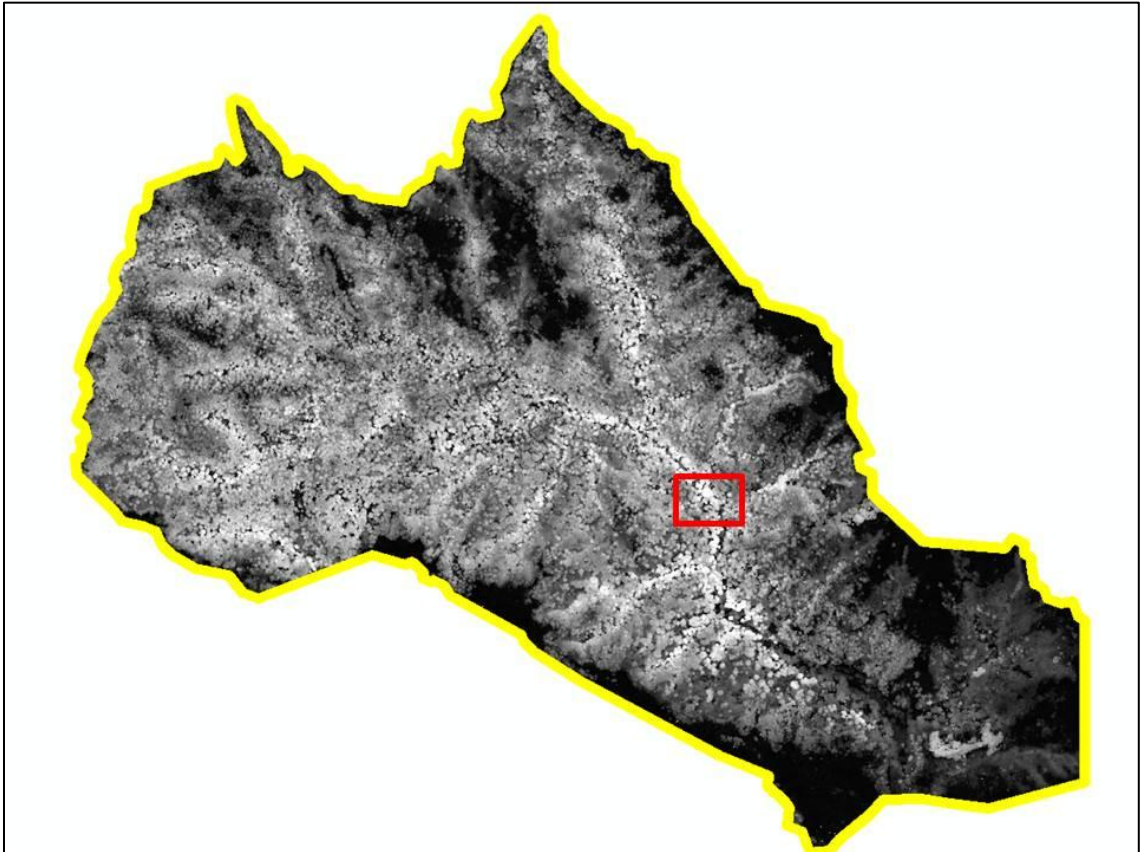


Figure 6: CHM clipped to Study Area.

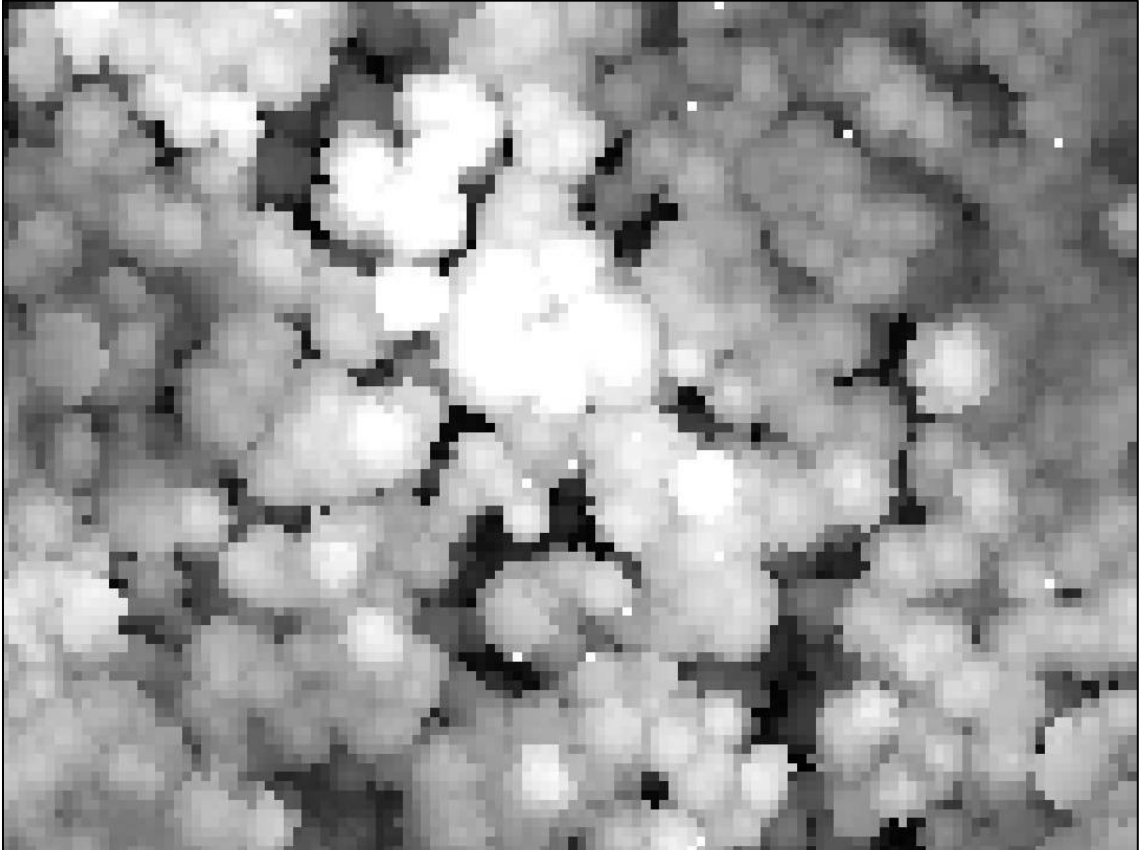


Figure 7: Close-up of clipped study area: Cathedral Grove in Muir Woods. Cathedral Grove is a cluster of old growth coastal redwoods; the oldest and tallest trees (shown in white) are found he

4.3 Field Work to Collect Training Data

To get a good measure of the intraspecies tree richness of this ecological landscape, random stratified sampling was used to collect the training samples (see Appendix 4 for a list of tools used). The stratified random sample, conducted in the summer of 2012, was broken into three sections:

- I. The southern section of Redwood Canyon, along Deer Park and Fire Road trails (see Figure 8). This section serves as an ecotone between chaparral and temperate rainforest, and is the warmest part of Redwood Canyon. Douglas firs dominate the uppermost canopy.
- II. Muir Woods. The main trails are the Ben Johnson, Bootjack, Fern Creek, and Hillside. Coastal redwoods dominate the upperstory canopy and the temperature is the coolest of three sections.
- III. The northern and eastern steep slopes of Redwood Canyon along the Panoramic Highway. The main trails are the Alpine, TCC, Troop 80, and Panoramic. Temperatures vary on these high altitudes; aspect and fog play a role in temperatures here. Coastal redwoods and Douglas firs dominate the uppermost canopy, and California bay laurels are present to a lesser extent.

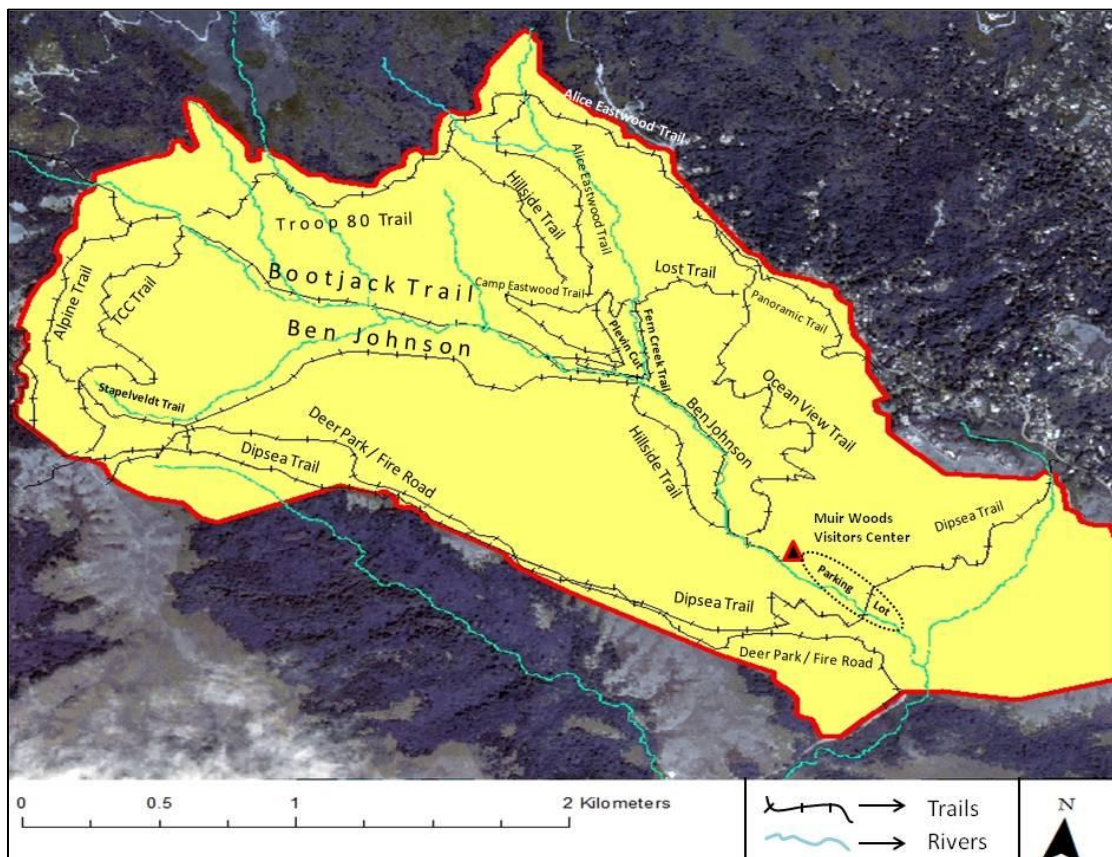


Figure 8. Trail Map of Muir Woods and surrounding Redwood Canyon.

The collection of training samples was affected by several factors. One is that the sampling is restricted to the parks trail system due to safety reasons. Additionally, the GPS receiver was incapable of generating a positional accuracy lower than a 5 meter error. As a result, Positional Dilution of Precision (PDOP) readings lower than 6 meters were chosen, even though PDOP usually averaged 5 meters in open areas. The high error could be caused by several factors, e.g. satellite to receiver signals bouncing off tree canopies, atmospheric effects (fog is common in this region), the multistory canopy, and

limitations of the GPS receiver (i.e. receiver clock errors). Collecting a training sample below a 6 meter error proved difficult. Because the error fluctuated sharply, a waiting of roughly 20 minutes was commonly necessary the error to go under 6 meters.

To reduce the multipath effect, training samples were predominantly collected adjacent to open areas. To help compensate for the high amount of positional error, a training point needed to be within a visually inspected large arboreal homogenous area (usually a 10x10m sq area) where identical trees also existed. Thus, there was a high degree of confidence that an identical tree will be chosen as a training point even though the positional error prevented identifying the exact tree where coordinates were extracted. Averaging the GPS position readings over time, and ensuring that at least 4 satellites were operational (to improve DOP), also helped in reducing positional error. In sum, the stratified random sample was not random at all, but more of a calculated stratified sampling that had to be imposed due to technological and logistical limitations.

A total of 147 training samples were collected. It was found that Redwood Canyon is dominated by only four main tree species. These four species are highlighted in Table 2 along with 6 other tree species which are also observed in Redwood Canyon. Because these four tree species dominate the area in terms of biomass and quantity, this research limits the classification to these four tree species only. It should be noted that, , though Tan Oak dominates the landscape in quantity similar to the 4 dominant trees species, is not included in sampling and classification because tan oak predominantly

inhabits the lowest section of the canopy. Its depiction is eliminated in the WV2 and CHM data.

Table 2. Trees of Redwood Canyon

Tree Species within Redwood Canyon
Big Leaf Maple (<i>Acer macrophyllum</i>)
Coastal Redwoods (<i>Sequoia sempervirens</i>)
California Bay Laurel (<i>Umbellularia californica</i>)
California Nutmeg (<i>Torreya californica</i>)
Coast Live Oak (<i>Quercus agrifolia</i>)
Douglas Fir (<i>Pseudotsuga menziesii</i>)
Interior Live Oak (<i>Quercus wislizeni</i>)
Red Alder (<i>Alnus rubra</i>)
Toyon (<i>Heteromeles arbutifolia</i>)
Tan Oak (<i>Lithocarpus densiflorus</i>)

Note: Dominant and most abundant trees are in red.

UTM coordinates for the training points (n = 147) were entered into an Excel spreadsheet and then transferred into ArcMap for plotting and visualization (Figure 9). Coastal redwoods (CR; n = 47) were sampled slightly more than Douglas fir (DF; n = 33), CA Bay Laurel (CBA; n = 35) and Coast Live Oak (CLO; n = 32) due to its dominance. Other noted trees were Big Leaf Maple (n = 6), Interior Live Oak (n = 2), California Nutmeg (n = 3), and Red Alder (n = 4).

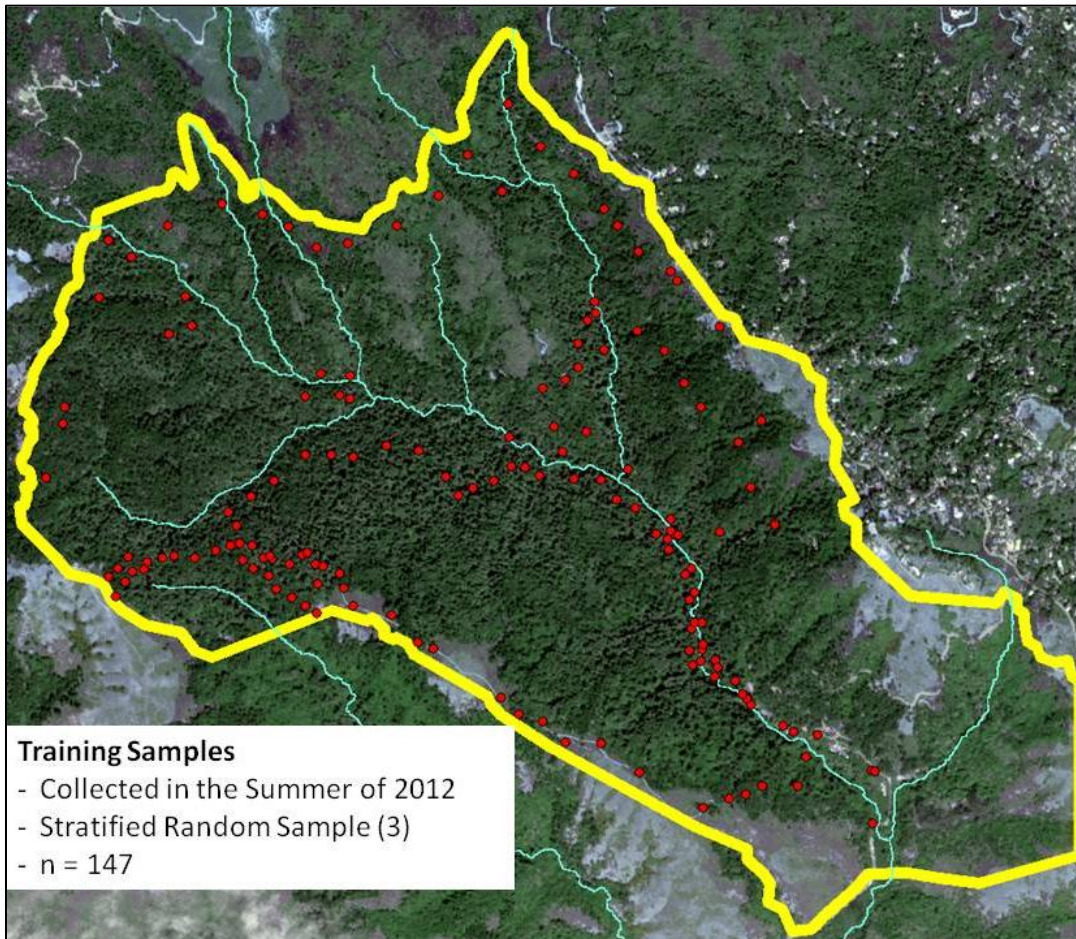


Figure 9. Training samples (n=147) in the study area. Training points were plotted in ArcMap 10.1. Note: red dots are training samples. Yellow outline is the extent of the study area. Light blue lines are rivers.

4.4. Object Based Image Analysis (OBIA)

The first step in the OBIA process is the segmentation of the image into objects using the multi-resolution segmentation (MS) within the eCognition software (2011, ver. 8.7). MS is a region-based iterative algorithm whereby pixels are grouped or merged together into homogenous objects --based on location, texture, shape, spectral similarities-- until a given threshold of upper variance is reached. The threshold for this bottom-up approach is the scale parameter; the scale parameter is also weighted with color, shape and compactness parameters (Darwish *et al.* (2003). The scale parameter is a variable that controls the maximum allowed heterogeneity within each object (Navulur 2007). The shape parameter is weighted between 0 and 1; the closer to 0 the more spectral color is pronounced, the closer to 1 then spectral color and object shape are more weighted. The compactness parameter symbiotically affects the shape parameter by either providing borders that are smooth or compact.

There was considerable difficulty in determining the appropriate scale parameter for the study area, as scholars vary in their approach. Voss and Sugumaran (2008) tested the scale parameter between 1 and 10 and results showed that a scale parameter of 3 produced the best accuracy for tree classification in Northern Iowa University. Ke *et al.* (2010) tested the effect of the scale parameter on accuracy for oaks, pines, and spruce trees in a New York State Park. The scales tested were 20, 50, 100, 150, 200, 250,

300, 400, 500, 600, 700, and 800. Results indicate that the best average accuracy was obtained with 250 for merged LiDAR-Multispectral, 200 for the multispectral data only, and 100 for the LiDAR data only. Yet accuracies for each tree varied widely for each different scale parameter. Hajek (2005) used a triple-level multiresolution segmentation scheme of 15, 5, and 3 for classifying a mixed deciduous forest. Novack *et al.* (2011) used a trial-and-error analysis in an urban setting (Sao Paulo, Brazil) to discover an appropriate multi-resolution segmentation scale parameter of 40; color parameter of 0.5, and compactness 0.7.

These studies suggest that choosing an appropriate scale parameter requires a trial-and-error approach by factoring in the study area and the objective of the study. The user has to inspect objects visually until the objects of interest are adequately and satisfactorily delineated. For this study, all the WV2 bands were given equal weights. A scale parameter of 12, a shape of 0.5, and a compactness of 0.2 were chosen because segmentation objects approximated single tree crowns and clusters of tree crowns the best with these parameters. Anything past a scale parameter of 12 resulted in objects so large that they encompass multiple trees. Anything under 12 resulted in objects too small to encompass a tree canopy.

The nearest neighbor (NN) classifier within eCognition, based on a fuzzy classification algorithm, was used. NN classification is more appropriate when classes are more difficult to separate from each other. This approach is better suited for evaluating

the correlations between object features and for describing a multidimensional feature space (Definiens, 2003, Laliberte *et al.* 2007). NN classified image objects may have a membership to more than one class, or between zero and one based on an object's feature space distance to its nearest neighbor. The smaller the difference is between sample objects and the object to be classified, the higher the association value. If a sample object differs from its neighbor, the feature space distance has a fuzzy dependency on the feature space distance to the nearest sample class. Hence, membership function at each point in the feature space is a combination of fuzzy functions over samples of the class being classified (Trimble 2011).

To define the four tree classes, samples obtained through the stratified sampling as described in section 4.3 were used. Training sites can be selected by double clicking on the sun-illuminated areas of the object (s) that corresponds to the training data. This trains the system to identify where each sample tree is located. eCognition then classifies the trained image objects based on their nearest sampled neighbors (Trimble 2011).

The Feature Space Optimized (FSO) tool in eCognition was used to evaluate the distance in the feature space between the samples in different classes. After training samples are collected, the tool selects the user defined features, or mean band values, that result in the best class separation distance; i.e. the FSO compares the spectral mean band values and finds the largest average minimum distance between the training samples of different classes (Definiens 2003, Laliberte *et al.* 2007). Object statistics of the

optimized feature space are calculated, bands are sorted on how well they separate classes, then their objects are classed based on the NN classifier (Platt and Rapoza 2008).

As shown in Table 3, the Distance Matrix shows a strong separability between Douglas Fir and CA Bay Laurel, and less strongly between Douglas Fir and Coastal Redwood. A value above 1 would suggest that the training samples separate the classes well (Definiens 2012), but the low "Best Separation Distance" of 0.194 suggests that the training samples do not provide good discrimination between the four tree classes. This is due to the similarity in spectral signatures between Coastal Redwood and Douglas Fir, between Coastal Redwood and Coast Live Oak, and between Coast Live Oak and CA Bay Laurel. The FSO-NN results also indicate that, in order of importance, the NIR2, Green, NIR1, Coastal, and Yellow bands are optimal (in terms of separability) in classifying the image. The FSO-NN algorithm then classifies the image; the output image (shown later) is used later for analysis with the LiDAR data.

The FSO procedure indicated that only 5 of the 8 bands provided the most favorable separability. This was an astonishing find, as the FSO procedure was able to identify the optimal bands with the best separability between the spectrally similar tree

Table 3. Class Separation Distance Matrix generated from the FSO tool.

Class	Coastal Redwood	Douglas Fir	CA Bay Laurel	Coast Live Oak
Coastal Redwood	0.000000	0.193834	0.375233	0.232727
Douglas Fir	0.193834	0.000000	1.570723	0.708994
CA Bay Laurel	0.375233	1.570723	0.000000	0.219426
Coast Live Oak	0.232727	0.708994	0.219426	0.000000

Note: Any distance closer to or higher than 1 indicates strong spectral separability between the two tree species.

classes. As shown in figure 10-18, there appear to be subtle yet noticeable spectral band differences between tree types within each band, especially in the Red Edge, NIR1, and NIR2 bands. Yet the Red Edge was excluded, and the Green, Yellow, and Coastal bands (which show spectrally similar radiance values) were included in the FSO. CA Bay Laurel's mean (red diamonds) and median values have a strong and distinguishable radiance value in the NIR1 band that sets it apart from the rest, but distinguishable tree differences can be found in each band, albeit minimal. A closer look suggests that mean and median spectral reflectance values for each tree class are similar in the Coastal band, so the FSO-NN 's inclusion of the Coastal Band is questionable. The Figures also show mean spectral differences in the Red Edge band which the FSO-NN classification deemed as ineffective in class separation.

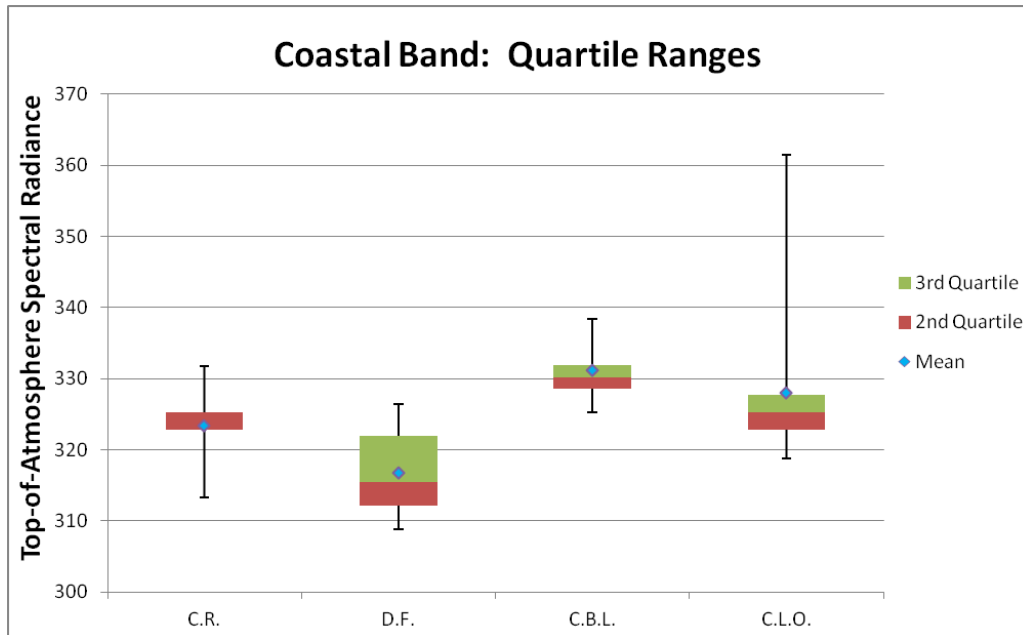


Figure 10. Quartile ranges of coastal band for each tree class. $n = 35$ per tree class. Note: C.R. = Coastal Redwood; D.F. = Douglas Fir; C.B.L. = California Bay Laurel; C.L.O. = Coast Live Oak. TOA spectral radiance is measured in units of $W m^{-2} sr^{-1} nm^{-1}$, where W is watts, m is meter, sr is steradian, and nm is nanometer.

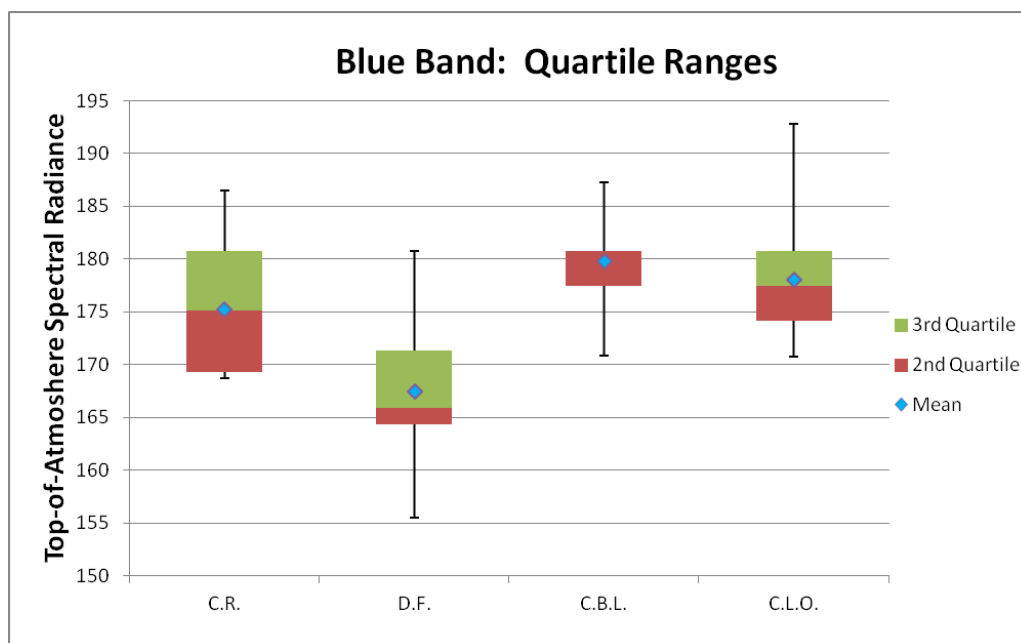


Figure 11. Quartile ranges of blue band for each tree class. $n = 35$ per tree class.

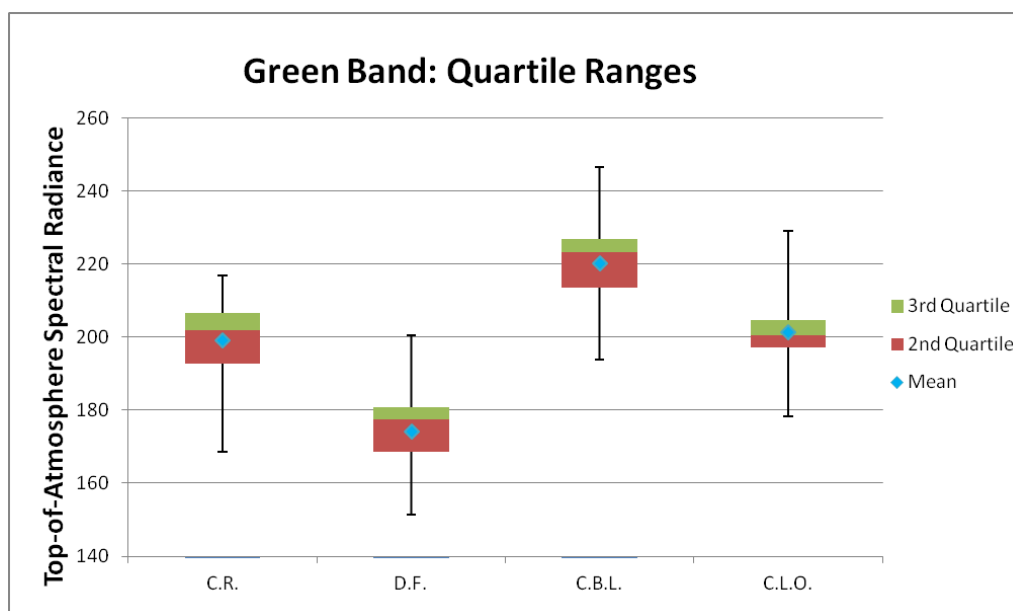


Figure 12. Quartile ranges of green band for each tree class. $n = 35$ per tree class.

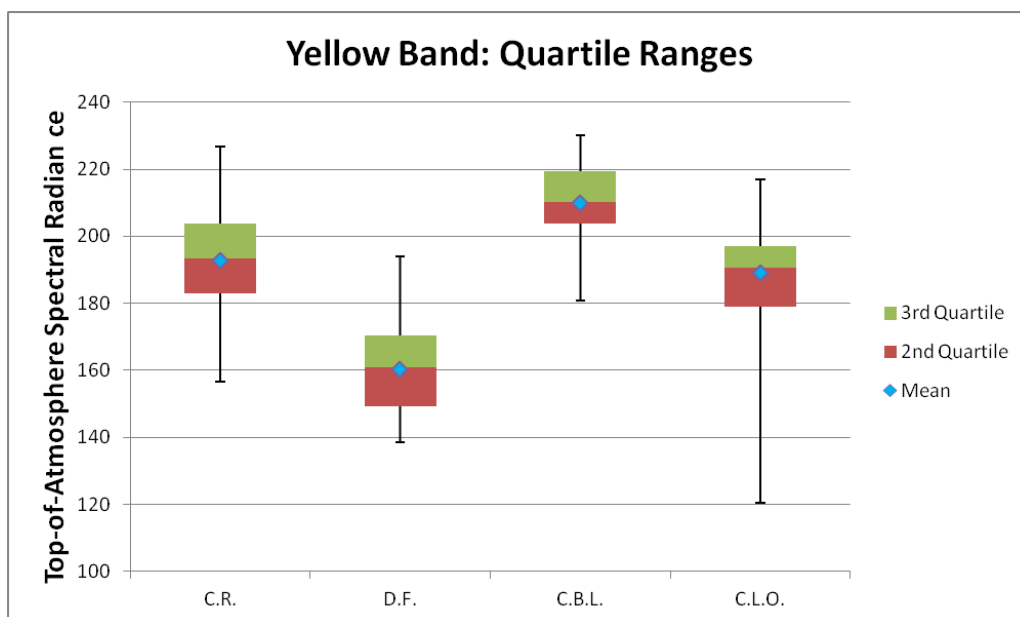


Figure 13. Quartile ranges of yellow bands for each tree class. $n = 35$ per tree class.

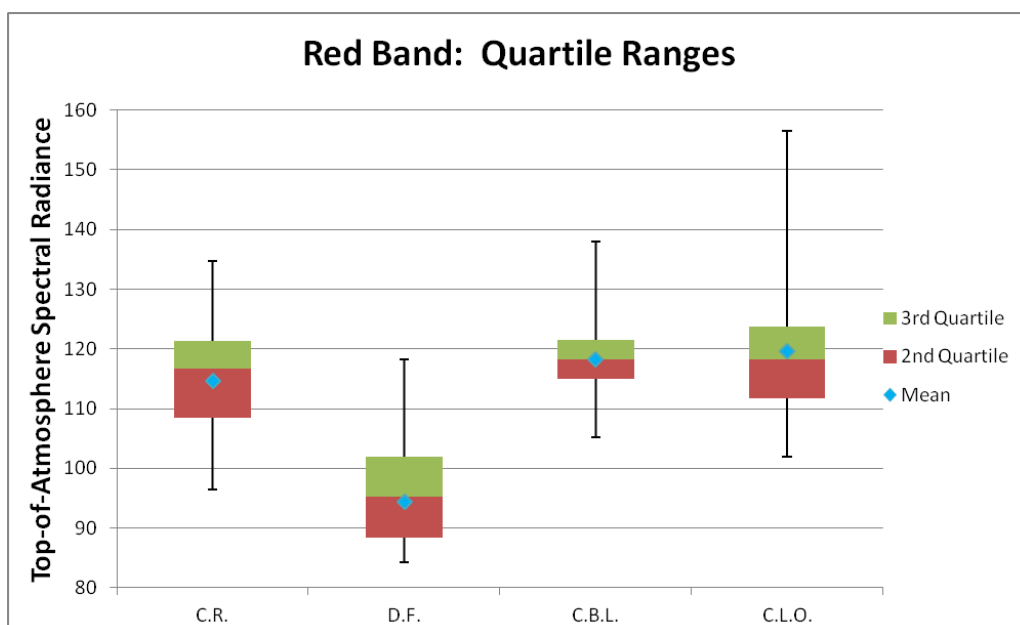


Figure 14. Quartile ranges of red band for each tree class. $n = 35$ per tree class.

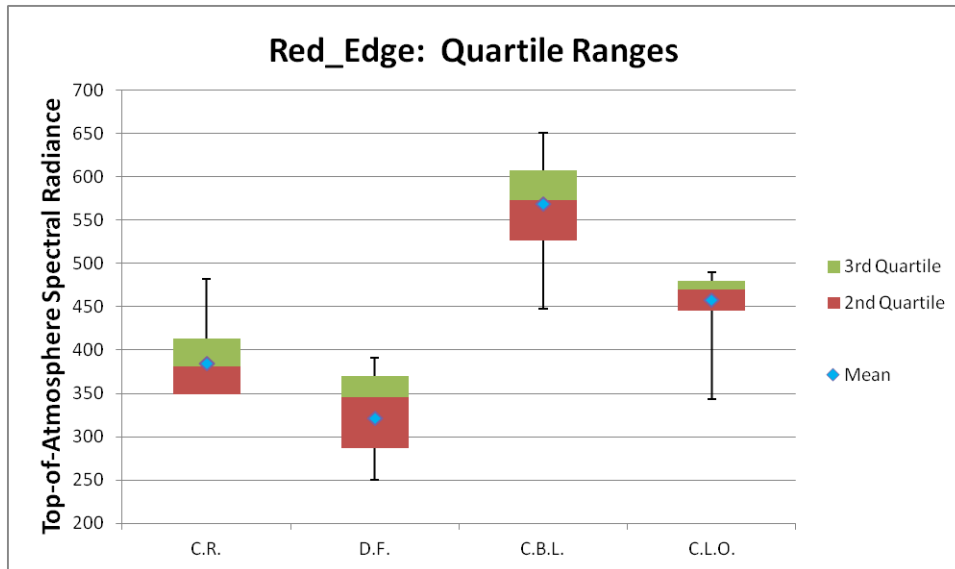


Figure 15. Quartile ranges of red-edge band for each tree class. $n = 35$ per tree class.

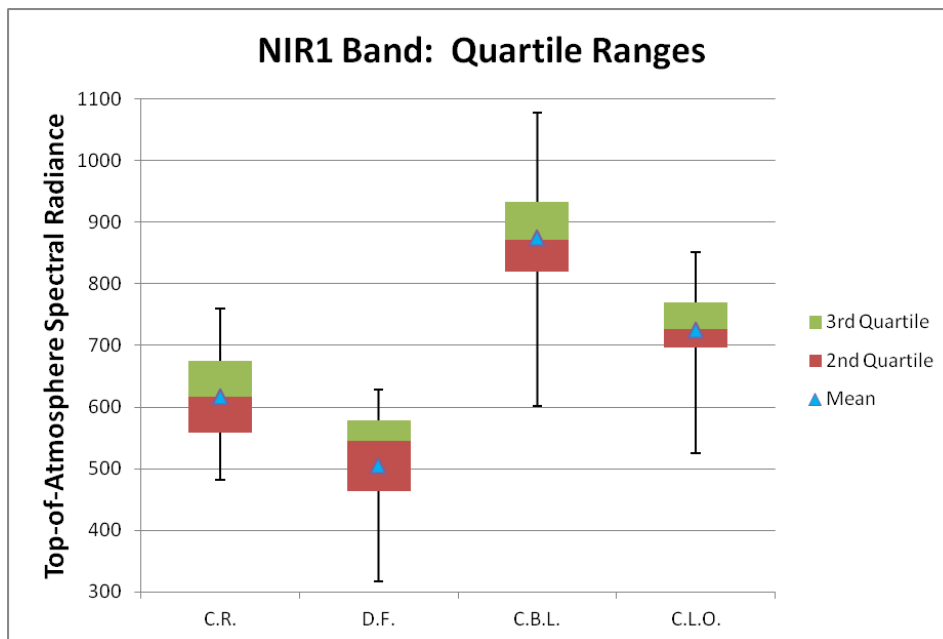


Figure 16. Quartile ranges of NIR1 band for each tree class. $n = 35$ per tree class.

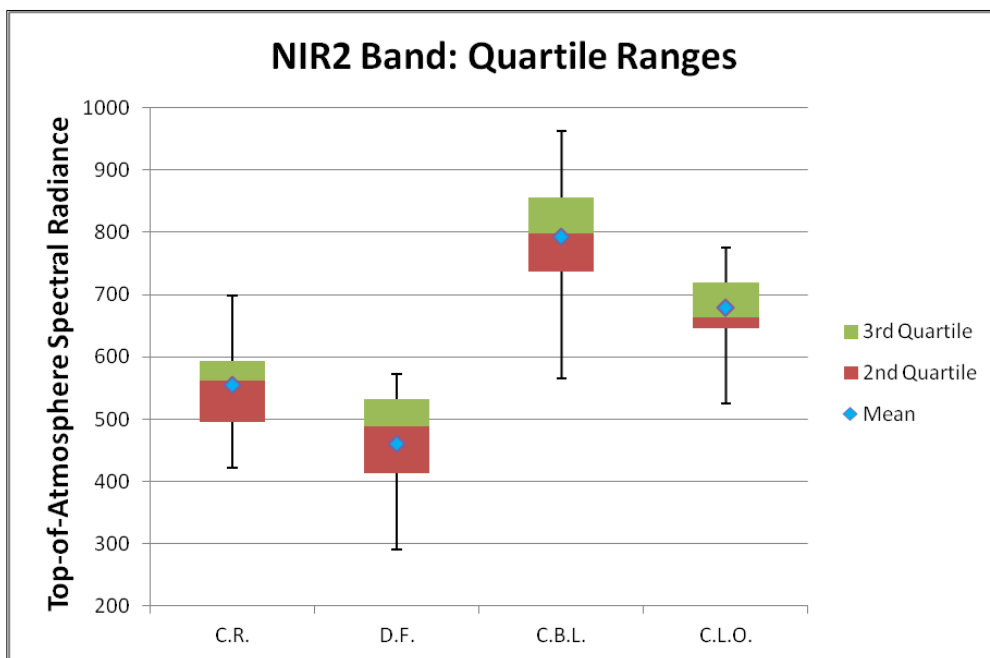


Figure 17. Quartile ranges of NIR2 bands for each tree class. $n = 35$ per tree class.

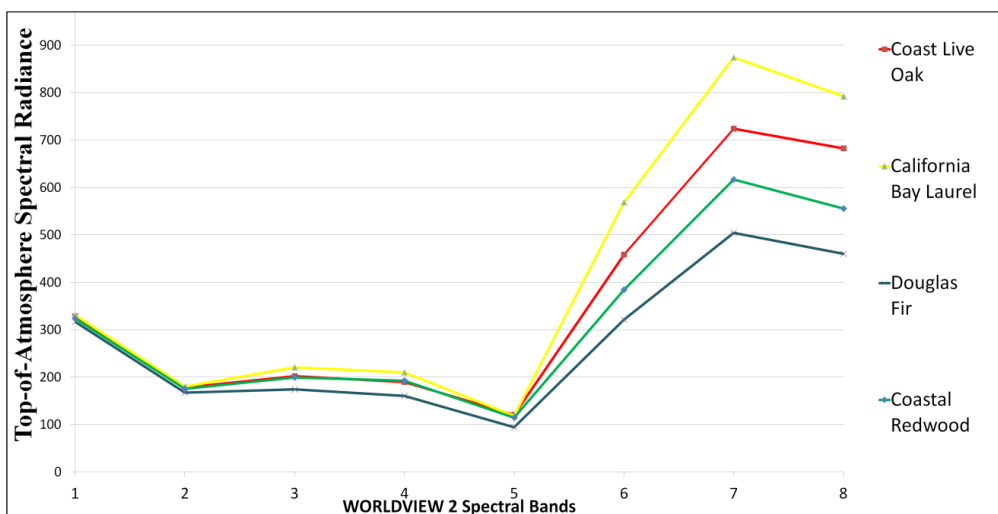


Figure 18. Mean spectral radiance profiles per tree class.

4.5. Maximum Likelihood Classification

The ML assumes a gaussian distribution of each class (Strahler 1980). It calculates the probability that a pixel is a member of a specific class using the mean and covariance of the training set. The ML classification was performed in Erdas Imagine 2011 using the Signature Editor tool. In similar fashion as the OBIA, Regions of Interest (ROI) were constructed from field data. ROI's or polygons were constructed over sunlit regions of trees identified from the training field data. The ROI regions were built, per class, to construct and classify signatures needed to perform the parametric classifier. For each class, excluding other insignificant classes (i.e. impervious surfaces, bare soil, grasses, shadows, and coyote bush), at least 500 pixels were used per class. Traditionally, the number of pixels to use per ROI is proportional to the number of bands in the image multiplied by 10. To remove salt-and-pepper effects, a 3x3 neighborhood majority filter was used on the output thematic layer.

4.6. Spectral Angle Mapper

SAM treats each spectrum, i.e. the reference spectrum (specified from the training data) and the observed spectrum (i.e. the random target cell to be classified) as vector in an n -dimensional scatter plot. " n " is equal to the number of bands in the image. The smaller the angle between reference and observed, the closer the relationship (Dennison *et al.* 2004, Shafri *et al.* 2007). The SAM classification was performed using the ENVI 5.0 software. Regions Of Interest's (ROI) were constructed from the ATCOR3 WV2

output (spectral radiance) in ENVI's classic module. ROI's were constructed in identical fashion as the ML classifier in Erdas Imagine, where sunlit regions of trees identified in the training field data are used. ROI's are used to extract endmember spectra (see Figure 16) which are subsequently used as input in the SAM classifier. Endmembers are spectra that are chosen to represent pure surface materials in a spectral image (Dennison *et al.* 2004, Shafri *et al.* 2007). The default Maximum Angle (radians) parameter of 0.3 was used as any value above or below 0.3 produces unfavorable results. Similar to the ML classifier, a 3x3 neighborhood majority filter was used on the output thematic layer to remove salt-and-pepper effects.

4.7 Problems Incorporating LiDAR

The incorporation of the LiDAR data to each classified image involved two different procedures. In eCognition, a rule set was built in order to define the mean CHM value to delineate each tree class for the NN classification. For the ML and SAM classification, the Knowledge Engineer tool within the Erdas Imagine 2011 software was used. The Knowledge Engineer interface is similar to the user defined rule set diagram of eCognition, except that Knowledge Engineer is less restrictive in the type of variables and parameters used.

At the start of this research, there was an assumption that the LiDAR data will help classification accuracies because it was commonly believed that Coastal Redwoods (CR) are the tallest trees in the Pacific Northwest. However, after gaining ground

knowledge of the area over a span of several months, the effectiveness of the CHM in helping improve classification results began to be questioned. As an alternative, other LiDAR-derived datasets, such as slope and aspect, began to be seriously considered as an alternative to the CHM. Based on the topographically varied nature of Redwood Canyon and ground knowledge, it was speculated that slope and aspect may play a role in determining the geographic location of each tree. In order to determine whether aspect, CHM, and aspect have any statistical significance in discriminating between tree species, several statistical tests were performed using a select number of trees (C.R., $n = 50$; D.F, $n = 47$; C.B.A. = 45; C.L.O = 45).

The first statistical test used was Multivariate Analysis of Variance (MANOVA) which is expected to answer whether the mean of a variable (i.e. CHM, slope, and aspect) is the same across tree classes. Since MANOVA requires homogeneity of variance, Levene's Test of Equality of Error Matrices was conducted. The p -value obtained for CHM is less than 0.05%, suggesting that the variances of CHM are not homogenous. A review of the Homogenous Covariance Matrix between the dependent variables and the tree types suggest that corresponding covariance values between tree types are 3 to 4 times greater than each other. This confirmation of unequal variances does not give power to the pursuit of the MANOVA tests. Further evidence against the use of MANOVA is provided by the Box's test of Equality of Covariance of Matrices which had a significant p value of less than 0.001%. This suggests that the observed covariance

matrices of the dependent variables (i.e. CHM, Aspect, Slope) are not equal across groups--a violation for an assumption of MANOVA.

Although not recommended, the MANOVA tests are continued with caution because MANOVA's is relatively robust against assumptions of the violation of homogeneity. In the "Tests of Between-Subjects Effects" table, across the four dependent variables, the MANOVA found statistically significant differences in slope ($p = 0.009$) and CHM ($p < 0.001$) between tree types. The use of Tamhane's T2 post hoc test (see the output Table 4 and 5), under the *Test Between-Subjects Effects* section of SPSS, conducts four separate t-tests (i.e. one for each tree type) between the three dependent variables (i.e. aspect, CHM, slope). This was done to investigate the individual mean differences on the two dependent variables that were statistically significant. The Tamhane's T2 post hoc test is usually performed when there is an assumption on the violation of homogeneity for MANOVA.

As shown in the Tamhane's tables for slope, when comparing the mean differences in slope between coastal redwoods (1) and coast live oak (4), there is a +/- 7.719 slope difference that is statistically significant at $p = 0.005$. When comparing the mean differences in CHM between redwoods and the other three trees, there is also a statistically significant differences between all the tree types. Since the MANOVA

Table 4. Tamhane's Test using Slope

Tamhane SLOPE	1.0 C. Redwood	2.0	2.903	2.3463	.773	-3.408	9.214
		3.0	4.583	2.5606	.381	-2.302	11.468
		4.0	7.719	2.2184	.005	1.733	13.705
	2.0 DouglasFir	1.0	-2.903	2.3463	.773	-9.214	3.408
		3.0	1.680	2.2200	.973	-4.299	7.658
		4.0	4.815	1.8146	.055	-.067	9.697
	3.0 CA Bay Laurel	1.0	-4.583	2.5606	.381	-11.468	2.302
		2.0	-1.680	2.2200	.973	-7.658	4.299
		4.0	3.136	2.0843	.586	-2.498	8.769
	4.0 CoastLive Oak	1.0	-7.719	2.2184	.005	-13.705	-1.733
		2.0	-4.815	1.8146	.055	-9.697	.067
		3.0	-3.136	2.0843	.586	-8.769	2.498

Table 5. Tamhane's Test using CHM.

Tamhane CHM	1.0 Coastal Redwood	2.0	22.636	3.2377	.000	13.942	31.331
		3.0	22.255	3.3912	.000	13.137	31.374
		4.0	33.826	2.8123	0.000	26.234	41.417
	2.0 DouglasFir	1.0	-22.636	3.2377	.000	-31.331	-13.942
		3.0	-.381	3.2148	1.000	-9.029	8.267
		4.0	11.189	2.5969	.000	4.192	18.187
	3.0 CA Bay Laurel	1.0	-22.255	3.3912	.000	-31.374	-13.137
		2.0	.381	3.2148	1.000	-8.267	9.029
		4.0	11.570	2.7859	.001	4.028	19.113
	4.0 CoastLive Oak	1.0	-33.826	2.8123	0.000	-41.417	-26.234
		2.0	-11.189	2.5969	.000	-18.187	-4.192
		3.0	-11.570	2.7859	.001	-19.113	-4.028

lacked robustness, due to the rejection of homogeneity of variances, this study chose to conduct more tests, particularly non-parametric tests. Conducting more tests aids in determining the validity or disuse use of the CHM and other datasets.

A CHI-Square test of independence, which required the need to convert CHM z-values and slope into categorical data (e.g. small, medium, tall, giant for the CHM; flat, medium, medium-high, steep for slope), was used to compare tree class with CHM and slope (Ho: CHM/slope is not related to tree type / Ha: CHM is related to tree type), and the resulting *p*-value of less than 0.001 for both CHM and slope indicate the probability of the model chi-square (477.97 for slope, 533.70 for CHM) fit was less than 0.001 for both variables. This suggests that the CHM and slope are good indicators of tree type; the null hypothesis that no difference exists between the tree variables and the models with CHM and slope was rejected. The existence of a relationship between tree type and the selected dependent variables is supported. The null hypothesis was accepted for aspect ($p = 0.099$), suggesting a weak relationship.

Through the use of SPSS, three more non-parametric tests were performed on the four tree classes: an independent samples median test (Figure 19), a Kruskal-Wallis test (Figure 20), and a Jonckheere-Terpstra test (Figure 21). The independent samples median test determines whether two or more populations have identical or very similar median values (Siegel 1988). The non-parametric Kruskal-Wallis test (equivalent to the parametric one-way ANOVA) is used to determine whether median differences between

two or more independent populations are identical or different --based on a variable of interest-- when ordinal, interval, or ratio level of data are available (Chan and Walmsley 1997, Kurskal and Wallis 1952). The null hypothesis states that the population medians are equal, whereas the alternative one-way ANOVA suggests differences between at least two means (Bewick *et al.* 2004). The Jonckheere-Terpstra test is identical to the Kruskal-Wallis test except when there *is* a natural *a priori* ordering (i.e. the height of trees, e.g. small, medium, tall) of independent populations. This test is preferable and more powerful than either the two former tests (Terpstra 1952, Jonckheere 1954). The results suggests that slope and CHM are not the same across tree type. Except for aspect, all the null hypotheses shown in Table 6 suggest that to a certain degree, CHM and Slope are related to tree type.

Additionally, yet another non-parametric test was performed: multinomial logistic regression (MLR). MLR is used to predict the probability of a categorical placement of a dependent variable based on multiple independent variables (Hosmer *et al.* 2013); it is used to analyze the strength of a relationship by classifying subjects (%) between a non-metric dependent variable (i.e. aspect, CHM, slope) and metric or dichotomous independent variables (i.e. tree type) (Hosmer and Lemeshow 2000). A tree is predicted to belong to a dependent variable associated with the highest percentage probability. Predicting tree class membership to an actual group membership is a measure of

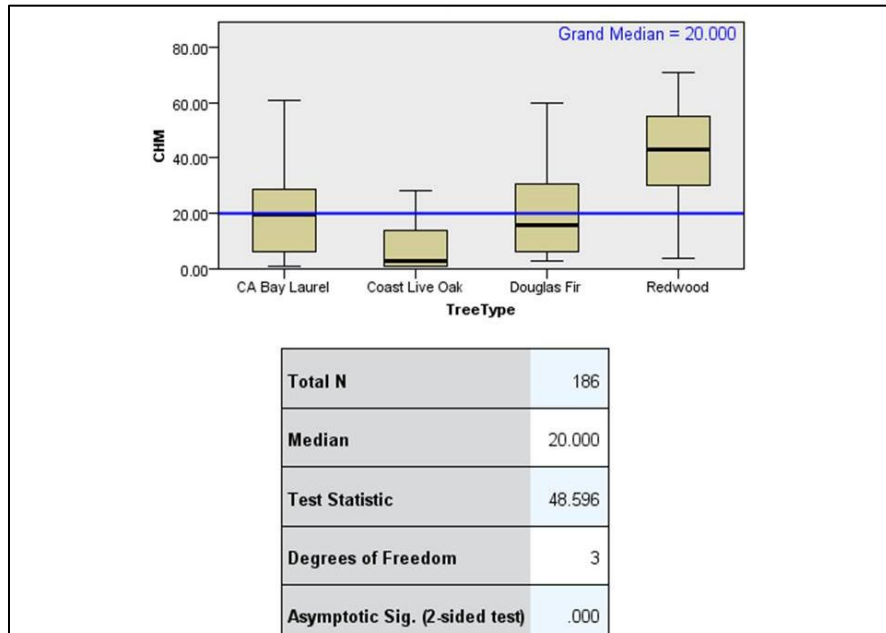


FIGURE 19. Independent-Samples Median test. Note: The vertical axis (CHM) is in meters.

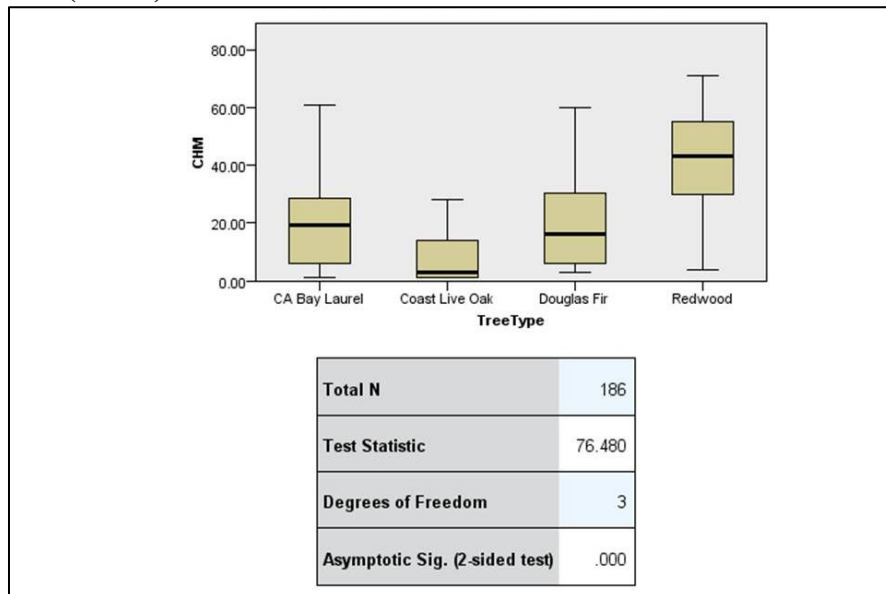


FIGURE 20. Kruskal-Wallis test of CHM

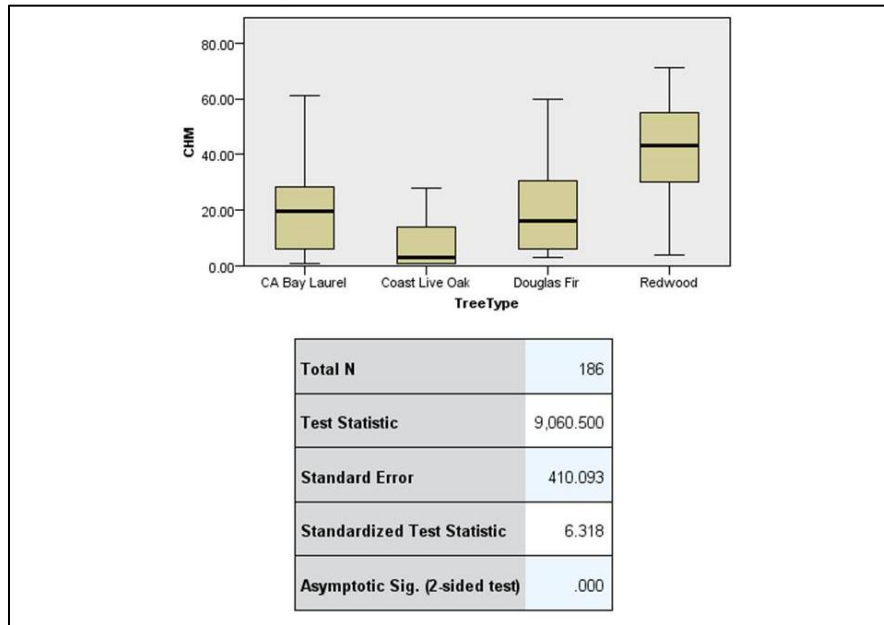


FIGURE 21. Jonckheere-Terpstra test for ordered alternative performed on CHM.

Table 6: Summary of Findings for employed Non-Parametric tests

Null Hypothesis	CHM	Slope	Aspect
Independent-n Median Test: The Medians are the same across the tree categories	Reject Null Hypothesis	Reject Null Hypothesis	Do Not Reject Null Hypothesis
Kruskal-Wallis Test: The Distributions are the same across the tree categories	Reject Null Hypothesis	Reject Null Hypothesis	Do Not Reject Null Hypothesis
Jonckheere - Terpstra: The Distributions are the same across the tree categories	Reject Null Hypothesis	Reject Null Hypothesis	Do Not Reject Null Hypothesis

classification accuracy. MLR does not necessarily abide by assumptions of normality of independent variables, linearity of relationships, equal dispersion matrices but it does require multicollinearity among independent variable (Bayaga 2010, Hosmer & Lemeshow (2000)).

Table 7 shows the results on using aspect, CHM, and slope together to classify 186 samples based on the MLR. The overall accuracy of all three variables is 46.8%. CHM by itself can differentiate tree type between the classes by 44.1% (see Table 8), slope with 37.6% (see Table 9), and aspect with 25.8%. (see Table 10), None of the MLR models are statistically significant. Supporting the results of the MLR is the "Likelihood Ratio" test; this test is normally conducted before the MLR. The Likelihood Ratio test suggested that the statistically significant relationship between tree type and aspect/slope was not supported.

Table 7. MLR Classification using CHM, slope, and aspect together

Observed	Classification				
	CA Bay Laurel	Coast Live Oak	Douglas Fir	Redwood	Percent Correct
CA Bay Laurel	9	15	12	8	20.5%
Coast Live Oak	5	26	9	1	63.4%
Douglas Fir	9	18	17	7	33.3%
Redwood	8	1	6	35	70.0%
Overall Percentage	16.7%	32.3%	23.7%	27.4%	46.8%

Table 8. MLR classification using CHM only

Observed	Classification				
	CA Bay Laurel	Coast Live Oak	Douglas Fir	Redwood	Percent Correct
CA Bay Laurel	0	16	20	8	0.0%
Coast Live Oak	0	27	14	0	65.9%
Douglas Fir	0	20	18	13	35.3%
Redwood	0	1	12	37	74.0%
Overall Percentage	0.0%	34.4%	34.4%	31.2%	44.1%

Table 9. MLR classification using slope only

Observed	Classification				
	CA Bay Laurel	Coast Live Oak	Douglas Fir	Redwood	Percent Correct
CA Bay Laurel	0	16	13	15	0.0%
Coast Live Oak	0	16	20	5	39.0%
Douglas Fir	0	8	28	15	54.9%
Redwood	0	14	10	26	52.0%
Overall Percentage	0.0%	29.0%	38.2%	32.8%	37.6%

Table 10. MLR classification using aspect only**Classification**

Observed	Predicted				
	CA Bay Laurel	Coast Live Oak	Douglas Fir	Redwood	Percent Correct
CA Bay Laurel	0	0	30	14	0.0%
Coast Live Oak	0	0	25	16	0.0%
Douglas Fir	0	0	30	21	58.8%
Redwood	0	0	32	18	36.0%
Overall Percentage	0.0%	0.0%	62.9%	37.1%	25.8%

No evidence of numerical problems in the models were found (the standard error was less than 2; this indicates no multicollinearity in the data), and the "estimate by chance" accuracy was 32%. Since the overall accuracy was 46.8% and higher than the "estimate by chance" accuracy, then the efficacy of the MLR model is proved. The best classification results, although statistically poor, comes through the use of CHM to identify tree type. The MLR also suggested that the CHM can classify each individual tree class with an accuracy of 55% (Coastal Redwood; CR), 25.5% (Douglas Fir; DF), 2% Coast Live Oak (CLO; 2%), and California Bay Laurel (CBL; 0%). The MLR also indicated that the California Bay Laurel is the most difficult tree class to differentiate using any dependent variable.

In sum, the statistical tests indicate a lack of strength in utilizing aspect, slope, and CHM to differentiate between the tree classes. Although the results of the MLR did

not find a statistically significantly categorical placement of CHM with tree type, the CHM will still be utilized nonetheless to strengthen the classification accuracy of CR. The rationale being that CRs have the highest mean and median z-values which can be distinguished from the other tree classes with an appropriate metric value. The difficulty lies in choosing a z-value (height) for CR that will not negatively affect the classification accuracy of the other tree classes. A trial and error approach was performed to test how the CHM improves (or impedes) the accuracy of CR (and the other tree classes) as CHM increases from 35m at 5 meter intervals. Beginning the trial-and-error approach at 35m was chosen as an arbitrary number.

4.8 Accuracy Assessment

To determine the appropriate quantity of reference sample points to collect per tree class, the following multinomial equation was used (Congalton and Green (2012):

$$N = B\varphi_i (1 - \varphi_i) / b_1^2 \quad [1]$$

where φ_i is the proportion of class closest to 50% (or 30% in this case), B is the upper percentile of χ^2 distribution with 1 degree of freedom ($k = 4$), and b_1^2 is the precision of confidence. In this study, a 90% confidence limit was used, thereby making B equal to 2.706 with the use of four classes. The equation generated a reference sample size of 73 per class.

Random reference points were collected through the guidance of the Accuracy Assessment (AA) tool in Erdas Imagine 2011. In the AA tool, the user has control over the amount of random points to generate. Using the ML classified image, over 5000 random points were generated per class in order to increase the probability of a random point falling within close proximity to roads and trails for verification. As previously mentioned, the study area can only be safely accessed by means of the established trail system. Within the established trail system, it is common to have near vertical +10m drops outside a 1m distance of a trail. Thus, safety was a key component in eliminating randomly generated AA reference points that were not located in close proximity to the trail system.

Another criteria for eliminating AA generated reference points is based on the probability of generating a high GPS positional error (over 6m positional errors were excluded; +20m error is common in the study area). A high GPS positional error prohibits the pinpointing of exact coordinates provided by the AA tool. Based on previously garnered knowledge of the study area (from the collection of training samples), it was known that certain areas generate high GPS positional error regardless of an open canopy. For these reasons center left sections of the study area are devoid of collected reference samples. Most reference points collected fall within areas where a reasonably good GPS positional error (between 5m - 6 m) can be extrapolated. Such areas fall on either the Kiosk/Parking lot area of Muir Woods, Dipsea Trail and Deer

Park/Fire Road, the north/south section of the Ben Johnson trail, and the Alpine/Alice Eastwood/Troop 80. Thus, AA generated reference samples went through a pattern of elimination that rested solely on the likelihood of producing high GPS positional error, and unsafe distances from the established trail system.

The AA random sample generation continued until 73 field-verified samples for each tree class was collected. All collected AA reference UTM coordinates were collected in an Excel spreadsheet and then imported into ArcMap 10.1 for visualization (see figure 22). For each classified map being generated, UTM coordinates (representing symbols) were overlaid to inspect the accuracy of the image and to subsequently generate error matrices in an Excel spreadsheet. User's and Producer's accuracy, as well as Kappa statistics were generated for each classified image.

In the field, the GPS receiver was a pivotal tool for determining the exact location of a reference sample given by the AA tool. Yet ground knowledge, the WV2 image, and Google Earth was equally useful for helping estimate the positional location of a reference point. Before the collection of reference points, the entire trail system of the study area had already been traversed. Furthermore, the 2 meter cell resolution of the WV2 image equates to a highly detailed image where the canopy structure of a given tree can be easily contrasted from other vegetation. With a reasonably good ground knowledge established, and with the highly detailed WV2 map for guidance, a reference point falling on a given tree canopy can be located in areas without a canopy cover along

the southern and northern areas of the study area. During field verification, the GPS receiver was used as the last process in confirming the location of a given reference point. This methodological process was practiced for collecting reference points along the Dipsea and Deer Park/Fire trails or along the southern boundary of the study area.

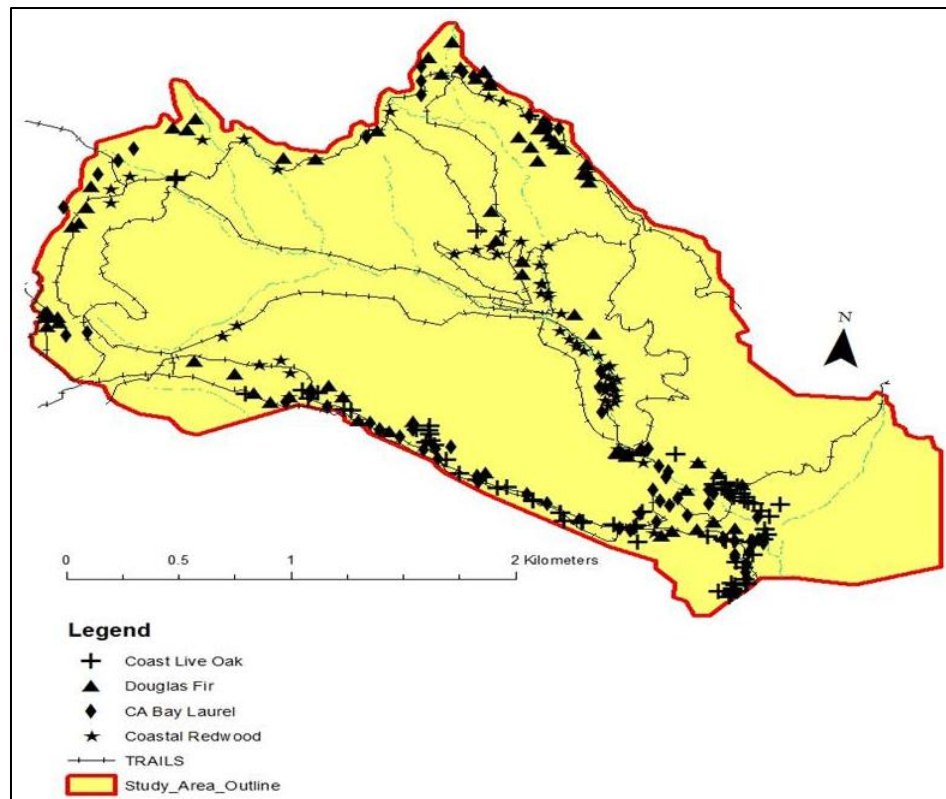


Figure 22. Distribution of training samples (n=297).

Google Earth's "street view" served as a strong visual aid for determining the location of AA random samples collected on the Alpine, Panoramic, and Troop 80 trails that are situated along the northern border of the study area. These trails are easily accessible by a vehicle because they are within a few meters of walking distance from the

Panoramic Highway. Before fieldwork was conducted, if a reference sample happened to fall in close proximity to trails that run parallel to Panoramic Highway, the "street view" option of Google Earth was utilized to visually inspect the area before conducting the field verification. This process involved printing a "street view" map as shown in figure 23, and using visual cues (i.e. road signs, unique trees or road features) within the image to determine where to stop and to specify the reference sample number to verify with the aid of the GPS receiver. Such time-saving pre-fieldwork preparatory steps was critical for knowing where to stop and inspect.

Based on the equation by Congalton and Green (2008) shown below, and the research by Ke *et al.* (2010), Kappa z-tests were used to determine whether Kappa values from two classifications are significantly different. With a null hypothesis of equal Kappa values, meaning the two Classifications are not significantly different from one another, the z-statistic was calculated as:

$$Z = \frac{k_1 - k_2}{\sqrt{\text{Var}(k_1) + \text{Var}(k_2)}} \quad [2]$$

Where k_1 and k_2 are the two kappa values, and $\text{Var}(k_1)$ and $\text{Var}(k_2)$ are their variances. If the z-statistic is greater than the critical value (1.96 for a 95% confidence level), then the null hypothesis will be rejected (Ke *et al.* 2010).



Figure 23. Example of Google Earth's "street - view." Note: visual cues as those shown in the figure were critical for faster collection of reference samples.

5. RESULTS

The FSO-NN classification provided the best accuracy (kappa 58%; Table 11), with the ML receiving 50% kappa (Table 12), and the SAM receiving 24% (Table 13). The FSO-NN provides a good representation of the study area (Figure 24), showing the non-uniformity of tree classes apparent in a mixed-conifer and evergreen temperate rainforest with various topographical differences. The image contrasts Coast Live Oak (CLO), California Bay Laurel (CBL), and Coyote Bush well, as these three classes are routinely found in close proximity to one another in the southern Dipsea trail boundary characteristic of chaparral vegetation.

Within the FSO-NN and SAM classification (Figure 25), CBL had a better producer/user accuracy than the other tree classes (FSO-NN%: 78/84%; SAM: 59/73%) while CLO fared the worst in all three (FSO-NN%: 58/74% (Table 11); ML: 55/58% (Table 12); SAM 34/42% Table 13)). Coastal Redwood (CR) received the worst accuracy with the SAM classifier (26/42%) as this class was routinely misclassified into Douglas Fir (DF), CLO, and Coyote Bush. The CR class in the FSO-NN classification provided the best accuracy (producer 71%/user 64%) compared to the ML and SAM.

The ML classification (Figure 26) over-classified CR along Troop 80 and Alice Eastwood trails. These trails have a mix of all the four tree classes, thereby negatively impacting user and producer accuracies for the CR class. Areas where CR is dominant,

Table 11. Confusion Matrix of FSO-NN

Reference Data. Feature Space Optimized-Nearest Neighbor Classification in eCognition					
Class Type from Classified Image	Actual Class				Row Total
	Coastal Redwood	Douglas Fir	CA Bay Laurel	Coast Live Oak	
Coastal Redwood	52	8	8	13	81
Douglas Fir	12	48	0	5	65
CA Bay Laurel	4	0	57	7	68
Coast Live Oak	5	6	4	40	55
Coyote Bush	0	3	4	8	15
Tree Shadows	0	8	0	0	8
Column Total	73	73	73	73	292

197

Producers Accuracy (rounded)	0.71	0.66	0.78	0.55
Users Accuracy (rounded)	0.64	0.74	0.84	0.73
Overall Accuracy (rounded)	0.67			
Kappa	0.58			

Note: Accuracy Assessment was only conducted on the four tree classes.

Table 12. Confusion Matrix of Maximum Likelihood (ML)

Reference Data. Maximum Likelihood Classification in Erdas Imagine					
Class Type from Classified Image	Actual Tree Class				Row Total
	Coastal Redwood	Douglas Fir	CA Bay Laurel	Coast Live Oak	
Coastal Redwood	45	18	12	12	87
Douglas Fir	16	44	0	2	62
CA Bay Laurel	4	1	49	8	62
Coast Live Oak	8	6	8	42	64
Coyote Bush	0	0	4	9	13
Tree Shadows	0	4	0	0	4
Column Total	73	73	73	73	292

Total 180

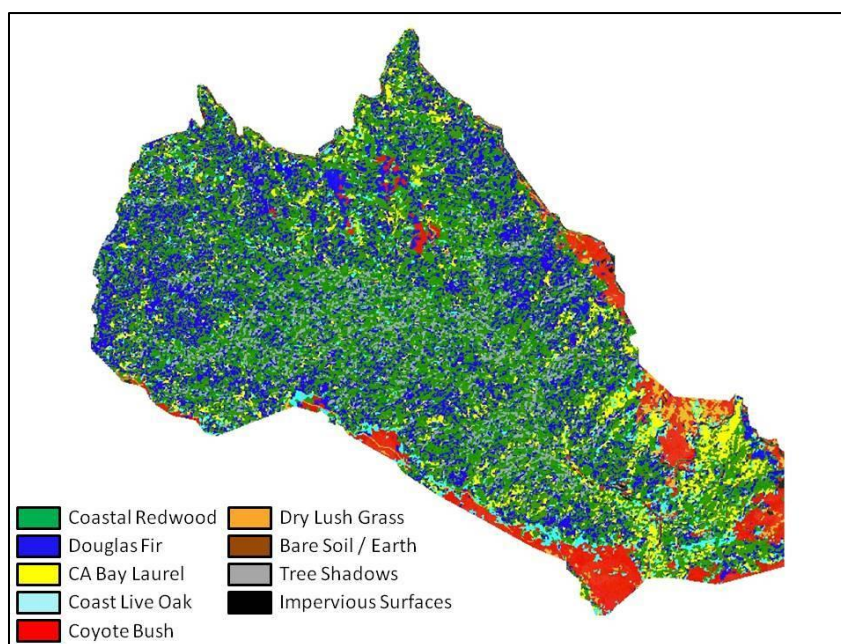
Producers Accuracy (rounded)	0.62	0.6	0.67	0.58
Users Accuracy (rounded)	0.52	0.71	0.79	0.66
Overall Accuracy (rounded)	0.6			
Kappa	0.5			

Table 13. Confusion Matrix of Spectral Angle Mapper (SAM)

		Actual Class				Row Total
		Coastal Redwood	Douglas Fir	CA Bay Laurel	Coast Live Oak	
Class Type from Classified Image	Coastal Redwood	19	9	6	5	39
	Douglas Fir	16	27	11	17	71
	CA Bay Laurel	3	5	43	8	59
	Coast Live Oak	12	14	8	25	59
	Coyote Bush	15	12	3	13	43
	Tree Shadows	8	6	2	2	18
	Dry Grass	0	0	0	3	3
	Column Total	73	73	73	73	292

114

Producers Accuracy (rounded)	0.26	0.37	0.59	0.34
Users Accuracy (rounded)	0.49	0.38	0.73	0.42
Overall Accuracy (rounded)	0.39			
Kappa	0.24			

**Figure 24. Classification of FSO-NN.**

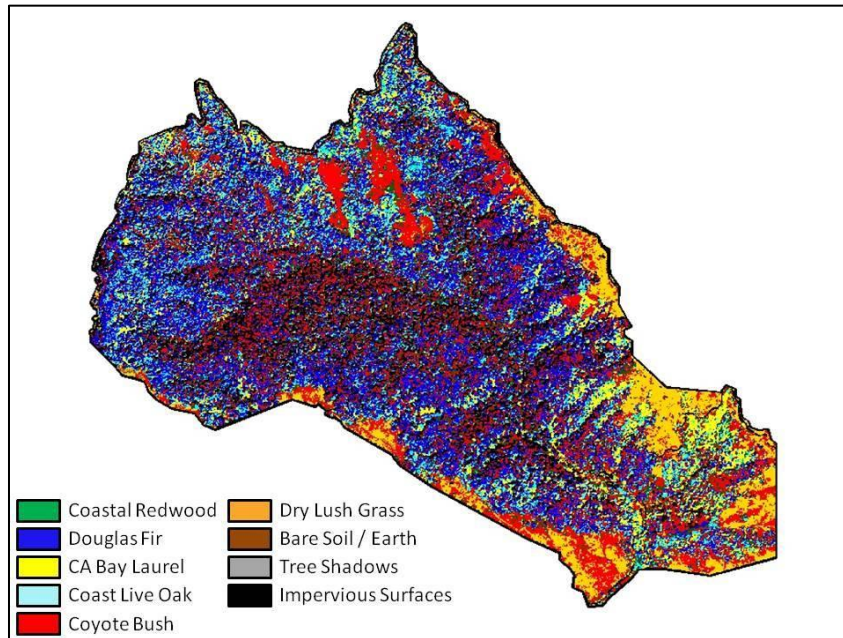


Figure 25. Classification of SAM.

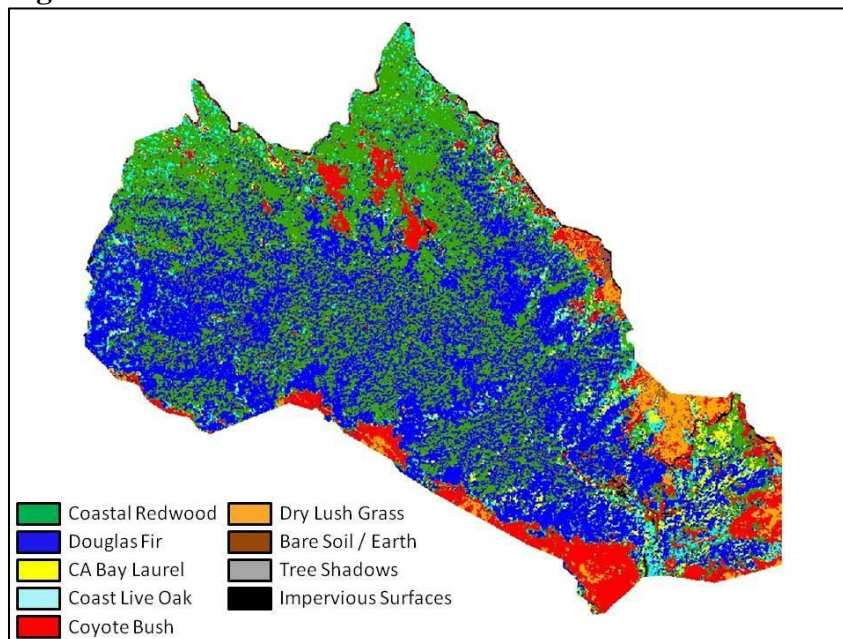


Figure 26. Classification of ML.

e.g. along the Ben Johnson and Hillside trail, have a spotted pattern of DL mixed with CR that further reduced accuracy. This pattern affects the FSO-NN as well although not as prevalent. The SAM classification showed poor results, as DF, CLO and Coyote Bush was routinely over-classified. DF was also regularly classified as impervious surfaces in the SAM classification.

As mentioned previously in section 4.7, a trial-and-error analysis was performed to test how the CHM improves or impedes the accuracy of CR (and the other tree classes) as CHM increases from 35m at 5 meter intervals. As shown in figures 27-29, similar mean and median CHM values between DF and CBL exist, and CHM ranges for any one

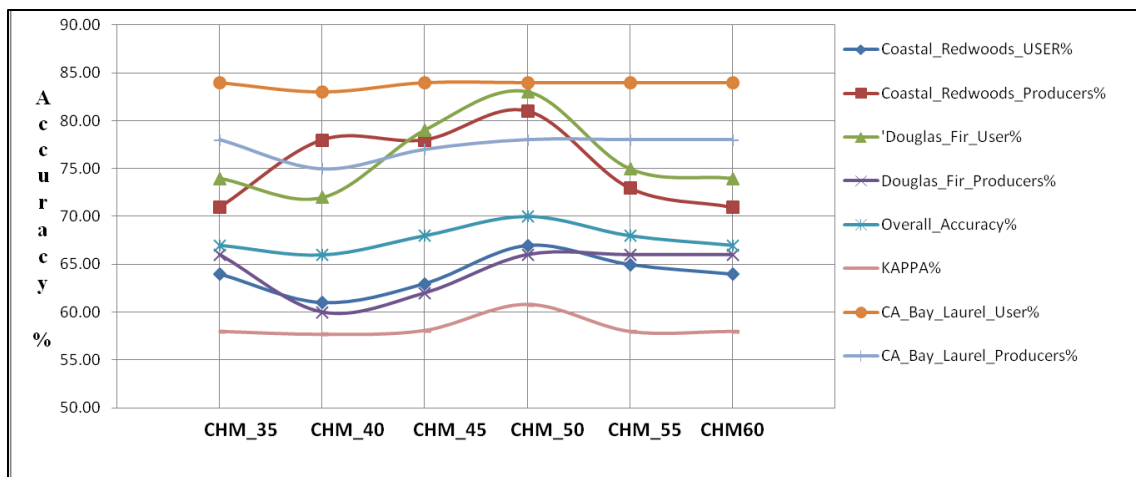


FIGURE 27. Trial-and-Error analysis as CHM increases from 35m in the FSO-NN classification.

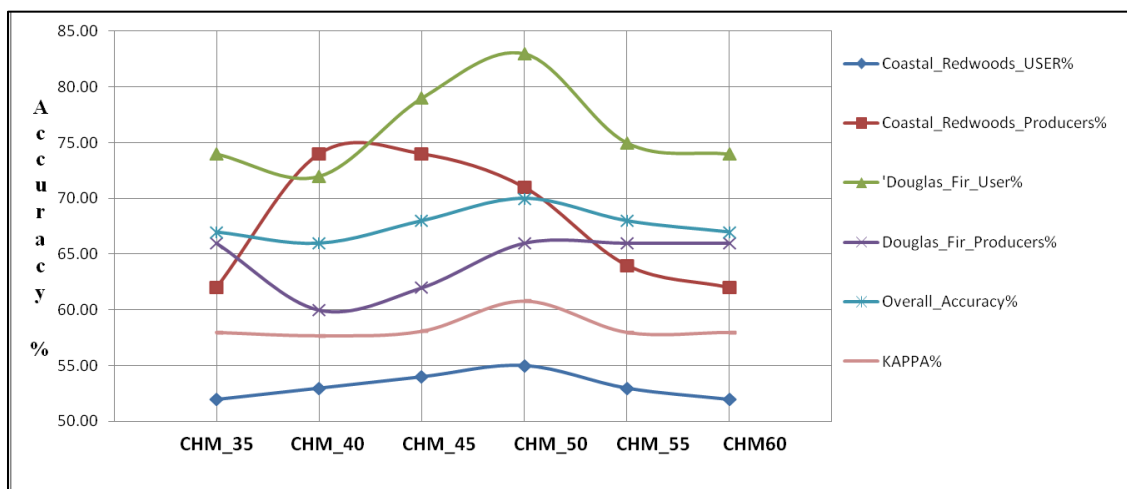


FIGURE 28. Trial-and-Error analysis as CHM increases from 35m in the ML classification.

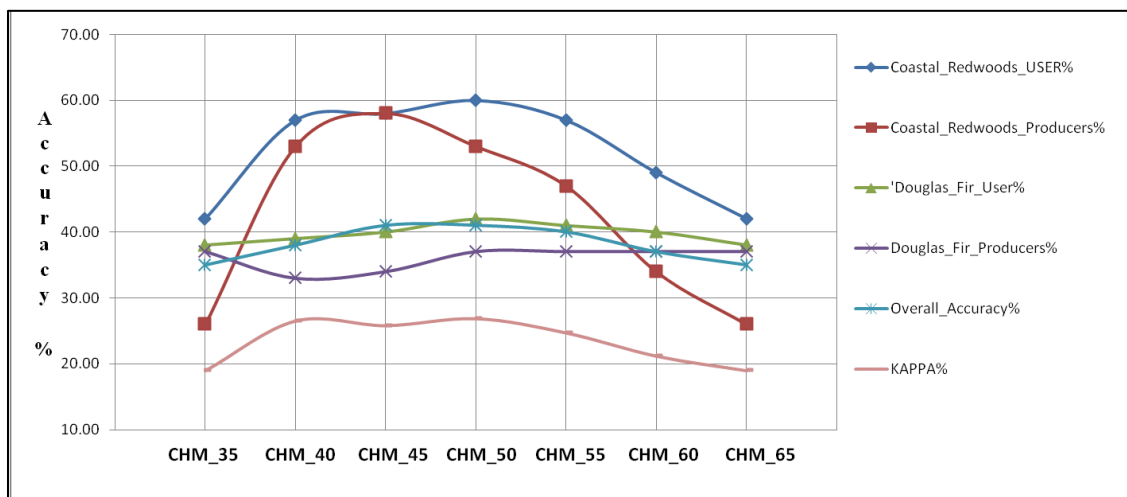


FIGURE 29. Trial-and-Error analysis as CHM increases from 35m in the SAM classification.

class traverse other classes. The statistical tests performed further implied a lack of statistical strength for utilizing the CHM to differentiate between the tree classes. Yet CR is the only class with the highest contrasting and median/mean CHM values than other tree classes, and therefore the analysis proceeded with caution for the CR class only.

Applying the CHM was made possible within the rule-based platform of Knowledge Engineer, a tool within Erdas Imagine 2011. The trial-and-error analysis began at 35m after a preview of results when CHM was applied lower than 35m significantly showed CR as being over-classified within areas know to be heavily DF (e.g. along the Alpine, Dipsea, Panoramic, and TCC trails).

With the introduction of the CHM, the Ben Johnson/Hillside trail becomes solid CR as CHM increases from 35m at 5m increments. Yet as shown in Figure 25-27, a CHM higher than 35m negatively impacts the DF class of all three classifications, albeit minimal, as the southwest section of the study area (Trails: Alpine, Dipsea, Deer Park, and TCC) is predominantly DF. A $CHM > 35$ negatively affects CBL for the FSO-NN classification. With a $CHM \geq 50$, negatively affected accuracies of DF and CBL return to their original condition while strong CR areas along the Ben Johnson trail become more solid CR. CHM becomes negligible as CHM reaches over 60m for the FSO-NN and ML classification, and when $CHM \geq 65$ for the SAM.

Applying $CHM \geq 50$ increases the FSO-NN by 3% kappa (Table 14, Figure 30), and the ML classification by 4% kappa (Table 15, Figure 31). The increase in accuracy

is attributed to an increase in robustness in the CR class along Ben Johnson/ Hillside trails where CR dominates. The CHM positively affects the CR in the SAM classification as well; kappa increases from 24% to 32% (Table 16, Figure 31). This relatively large increase is attributed to the poor CR results in the SAM classification; CR was routinely misclassified as coyote bush, DF, and CLO throughout the map but the CHM corrects some of these misclassifications back to CR. A summary of results given by the error matrices is given in Table 17.

Table 18 represents the z -statistic results for testing the significant differences amongst two matrices. The z-statistic for comparing matrices determined that the ML-CHM (52% kappa) and SAM-CHM (32% kappa) classifications suggest statistically significant differences. As evident from the error matrices and images comparing OBIA-CHM (62% kappa) and ML-CHM, z-statistic results confirm no statistical significant differences even though there is a 8% kappa difference between them.

Table 14. Confusion Matrix of FS0-NN with CHM ≥ 50

**Reference Data. Feature Space Optimized-Nearest Neighbor Classification
w/50 CHM**

	Actual Class				Row Total
	Coastal Redwood	Douglas Fir	CA Bay Laurel	Coast Live Oak	
Coastal Redwood	59	8	8	13	88
Douglas Fir	5	48	0	5	58
CA Bay Laurel	4	0	57	7	68
Coast Live Oak	5	6	4	40	55
Coyote Bush	0	3	4	8	15
Tree Shadows	0	8	0	0	8
Column Total	73	73	73	73	292

204

Producers Accuracy (rounded)	0.81	0.66	0.78	0.55
Users Accuracy (rounded)	0.67	0.83	0.84	0.73
Overall Accuracy (rounded)	0.7			
Kappa	0.61			

Table 15. Confusion Matrix of Maximum Likelihood with CHM ≥ 50

Reference Data. Maximum Likelihood Classification >50 CHM

	Actual Tree Class				Row Total
	Coastal Redwood	Douglas Fir	CA Bay Laurel	Coast Live Oak	
Coastal Redwood	52	18	12	12	94
Douglas Fir	9	44	0	2	55
CA Bay Laurel	4	1	49	8	62
Coast Live Oak	8	6	8	42	64
Coyote Bush	0	0	4	9	13
Tree Shadows	0	4	0	0	4
Column Total	73	73	73	73	292

Total 187

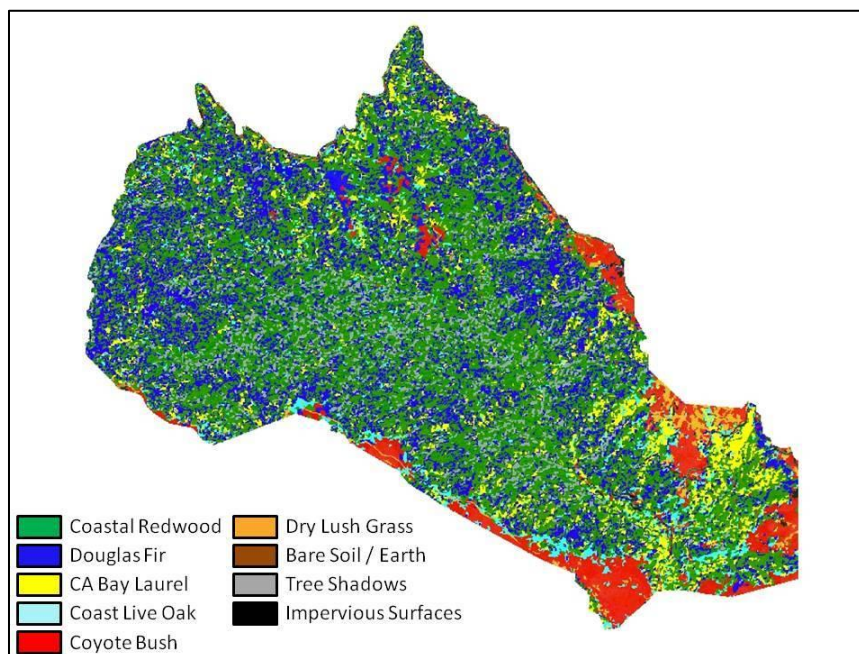
Producers Accuracy	0.71	0.6	0.67	0.58
Users Accuracy	0.55	0.8	0.79	0.66
Overall Accuracy	0.62			
Kappa	0.53			

Table 16. Confusion Matrix of Spectral Angle Mapper ≥ 50

		Actual Class				Row Total
		Coastal Redwood	Douglas Fir	CA Bay Laurel	Coast Live Oak	
Class Type from Classified Image	Coastal Redwood	39	9	6	5	59
	Douglas Fir	9	27	11	17	64
	CA Bay Laurel	3	5	43	8	59
	Coast Live Oak	6	14	8	25	53
	Coyote Bush	8	12	3	13	36
	Tree Shadows	8	6	2	2	18
	Dry Grass	0	0	0	3	3
	Column Total	73	73	73	73	292

Producers Accuracy (rounded)	0.53	0.37	0.59	0.34
Users Accuracy (rounded)	0.66	0.42	0.73	0.47
Overall Accuracy (rounded)	0.46			
Kappa	0.32			

134

**FIGURE 30. Classification of FSO-NN with CHM ≥ 50**

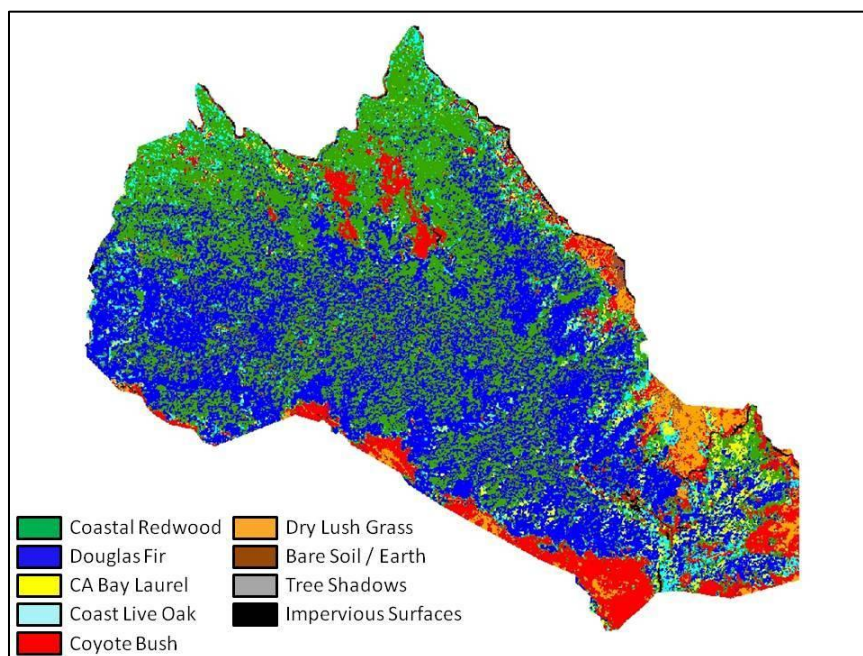


FIGURE 31. Classification of SAM with CHM ≥ 50

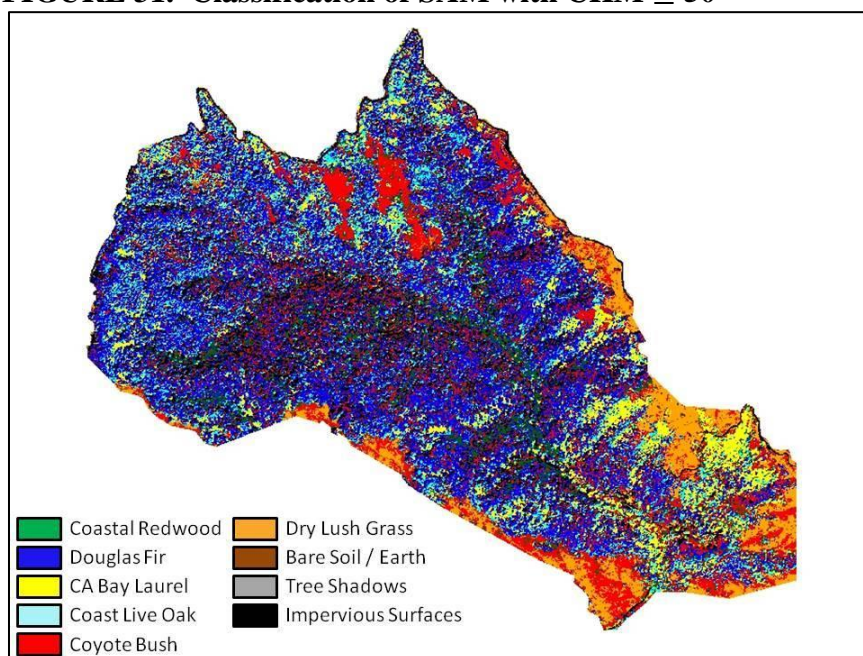


FIGURE 32. Classification of SAM with CHM ≥ 5

Table 17. Summary of classification results

Summary of Results		
Classification	Overall Accuracy (%)	Kappa (%)
FSO-NN	68	59
FSO-NN + CHM ≥ 50	71	62
ML	60	50
ML + CHM ≥ 50	62	53
SAM	39	24
SAM + CHM ≥ 50	46	32

Table 18. Summary of z-statistic results

Test of Significant Differences between Error Matrices	
Comparison	z - Statistic
SAM (CHM ≥ 50) vs ML (CHM ≥ 50)	3.69*
FSO-NN (CHM ≥ 50) vs ML (CHM ≥ 50)	1.62**
FSO-NN (CHM ≥ 50) vs SAM (CHM ≥ 50)	5.49*

* significant at the 95% confidence level (1.96). ** NS = Not Significant

6. Discussion

The results are indicative of a slightly modest improvement in classification accuracy when the CHM is incorporated, but only specific to the CR class. If specifying the CHM under 50m, classification accuracies affect the DF and CBL class, albeit minimal. Accuracy improvement began to diminish as CHM was specified to extract CR over 55m. Results also are indicative of better classification results of the OBIA using the FSO-NN procedure.

Results proved significant for the CBL class, as all classification outputs were very successful in delineating CBL tree amongst the other tree classes. An explanation can be sought in the feature space image shown in Figure 33. Figure 33 displays CBL as being predominantly positioned in the highest section where vegetation cohabits in n -dimensional space. Also noted is the compactness of all vegetation classes in one section of the feature space; this sheds light on the difficulty of the classifying algorithms, especially the SAM, to differentiate these spectrally similar tree classes. It also sheds light on the strength of the FSO-NN/OBIA in providing a good discrimination of spectrally similar tree classes.

At the pixel scale, ML generally had higher overall accuracy and Kappa than SAM using all 8 bands and sunlit-only pixels. SAM had very low performance, with an insignificant Kappa accuracy below 35%. The modest underperformance of the ML classification is possibly due to a lack of a sufficiently Gaussian distribution, resulting in

a poor representative description of the respective tree classes. This is not surprising, considering the wide in-class spectral variation (as shown in figure 33) that is further compounded by tree shadows.

The SAM classifier was the least successful of the classifiers, even with the incorporation of the CHM. Although SAM is relative insensitive to brightness or solar illumination factors (Petropoulos *et al.* 2010), poor results can be explained by a lack of second-order statistics (e.g., covariance), and its reliance on a single distance metric that appears ineffective given intra-species spectral diversity in a forest stand (Clark *et al.* 2005).

It is believed that the FSO-NN Classification performed well in part by the utilization of an appropriate scale parameter, through a trial-and-error approach, that culminated in a WV2 segmented image at small scales that closely resembled forest stands. This approach inadvertently also accurately separated and distinguished shadows and gaps from sun-lit tree crowns. With the integration of the CHM in the multi-resolution segmentation, the CHM possibly further helped mitigate the shadow effect in areas where tree heights were homogenous. As Ke *et al.* 2010 suggests, the LiDAR derived CHM is not influenced by relief displacement and shadow effects.

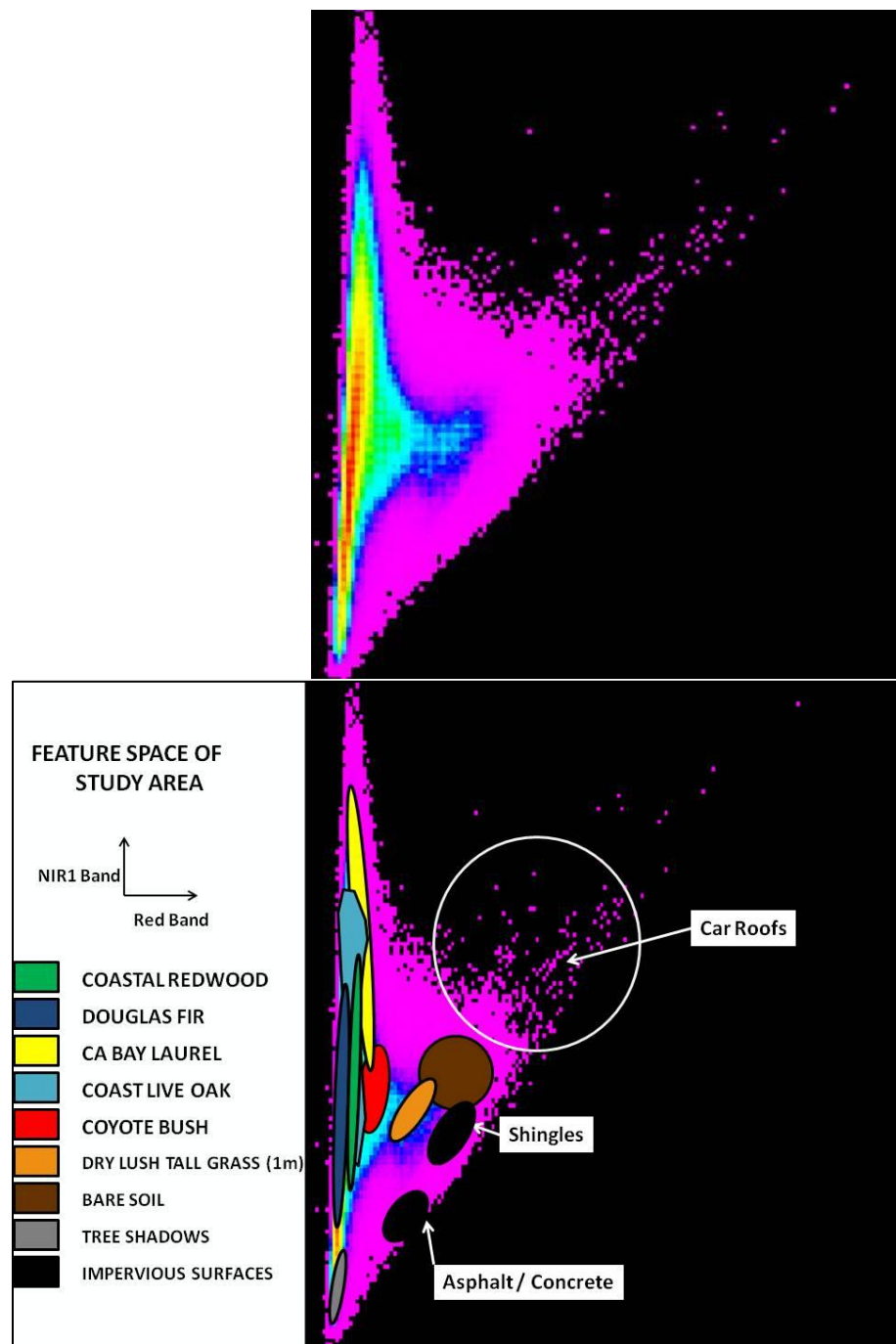


FIGURE 33. Feature Space of Study Area

Other reasons the FSO-NN performed well is the lack of the salt-and pepper phenomenon that is more common in PBC. The ML and SAM continued to modestly exhibit salt-and-pepper effects even after a 3x3 neighborhood majority filter was employed. Yet a large factor for the FSO-NN's relatively good kappa accuracy rests on its use of the fuzzy classification algorithm which appears to be better suited for evaluating spectrally similar classes (Laliberte *et al.* 2007), and the utilization of optimized bands (NIR2, Green, NIR1, Coastal, and Yellow bands) via the FSO tool in eCognition.

7. Conclusion

Studies using a multi-sensor and OBIA approach in a Northwestern Pacific temperate rainforest environment are lacking. This research evaluated the synergistic use of high spatial resolution multispectral data and a CHM created from LiDAR point cloud data in a highly topographically varied and temperate rainforest environment of the Pacific Northwest. The results from an OBIA approach using the WV2 optical sensor was compared with pixel-based ML and SAM classification. Subsequently, the CHM was synergistically used in all three classifications and the results were compared.

It is difficult to compare these results with other studies using the WV2 sensor and LiDAR for tree species identification. Different study sites, optical sensors, tree species, number of tree classes, seasons, and the sampling designs vary by study (Keempeneers *et al.* 2009). The WV2 sensor is still relatively new and few studies have been carried out to test its efficiency in forest mapping using OBIA (Ozdemir and Karnieli 2011, Zhang *et al.* 2012b). The only comparable study was conducted by Zhang *et al.* (2012b) in a mixed evergreen temperate rainforest of Australia. Zhang *et al.* (2012b) similarly used airborne LiDAR (at 4 returns per laser pulse) and all WV2 bands in a CART decision tree classifier. Results showed that the combined use of both datasets exhibited more discriminatory power for five tree species. Overall accuracy was 82%, and kappa was 77%.

The statistical analysis in this study revealed that the usage of the CHM was not strongly supported, primarily due to similar mean heights particularly between these four tree classes. However, it was found that the CHM is most effective, albeit minimal, in classifying the CR class which has moderately but significantly higher mean and median CHM values than other tree classes. A trial-and-error approach revealed that Kappa results improved when assigning all CHM values equal-or-greater than 50m to the CR class. Anything lower than 50m increases the chance that DF and CBL classes are misclassified as CR.

As suggested by the scientific literature, the kappa results indicate that the OBIA, through the use of the multi-resolution segmentation and feature-spaced optimized classification, offers the best accuracy over the ML and SAM classifications. The inclusion of the LiDAR point cloud, in the form of a CHM, improved Kappa results for all classifications by boosting the accuracy of the CR class, albeit minimal by an average of 4.6%. Similar results were discovered by Dalponte *et al.* (2009), Geerling *et al.* (2007), Jones *et al.* (2010), and Ke *et al.* (2010) when LiDAR was applied in arboreal classifications. The z-statistic for comparing matrices determined that the ML-CHM (52%) and SAM-CHM (32%) classifications are significantly different, but not between the OBIA-CHM (Kappa 62%) and ML-CHM classifications even though the Kappa for the OBIA-CHM is 8% higher.

If given the choice of utilizing only these two approaches (i.e OBIA-CHM and ML-CHM), one could argue for the easiest and most efficient approach because the accuracy may not differ too much. Yet from the perspective of conducting this research, the difficulty in utilizing both approaches are similar, along with computational requirements. Therefore the OBIA-CHM approach is favored for its better accuracy in more accurately representing the environment under study. Thus, an OBIA for forest species classification and inventory in topographically heterogenous and species rich forests of the Pacific Northwest is most creditable of further investigation, but caution is advised when utilized a CHM in conjunction with optical imagery due to similar inter-species tree heights and spectral signatures.

Ozdemir *et al.* (2011) argues that spectral information alone is generally not sufficient for detailed forest mapping. They discovered that relations between first order texture (standard deviation of gray levels) and structural parameters, i.e. basal area and stem volume, are variables that are positively associated with canopy cover type in plantation forests where trees are planted at regular intervals. Although such variables may not have a strong association with canopy cover type in a natural old growth temperate rainforest of the Northwest Pacific coast, Ozdemir *et al.* (2011) believe an OBIA should consider texture variables such as homogeneity, dissimilarity, angular second moment, correlation, and those based on Gray Level Co-occurrence Matrix (GLCM) for improved forest mapping.

The tree shadow effect, caused by trees of varying height, sun angle, and topography within close proximity to each other, further compounded misclassification. Although tree shadow was easily classified and was placed in its own class, such a class only represented dark black tree shadows, not a wide spectrum of shadow color and texture. Depending upon the amount of shadow incident upon a tree by another, the spectral range per band of a given tree can fall within the range of other tree classes more profoundly, as pixels within a tree crown will display varying illumination. Thus, it is probable that tree shadows was a main contributor of confusion in tree classification, as CR was repeatedly confused as DF in all classifications.

Zhang *et al.* (2011) discovered that topographic correction methods (i.e. Cosine correction, Minnaert correction, C-correction, Sun-canopy-sensor correction, two-stage topographic normalization, and slope matching technique) actually decreased oak and mixed forest accuracies using corrected images in the rugged mountainous terrain of Southern China. For more profound forest mapping of the Pacific Northwest, future research has to strongly consider the negative effect of tree shadows for accurate forest mapping by improving upon available topographic normalization techniques.

The FSO-NN procedure has not been previously used in forest applications. This non-parametric rule, independent of a normal distribution, has been applied in both urban (Myint et al 2011) and arid (Liliberte *et al.*2007) environments. Due to better results over the ML and SAM classifications, parametric classifiers should be avoided. Future

research should consider testing several different non-parametric classifier in Pacific Coastal rainforests. Decision tree and support vector machine (SVM) are attractive classifier models to test; they are increasingly being used in conjunction with OBIA because they are non-parametric methods, which require no assumptions for data distribution and feature independency (Ke *et al.* 2010).

8. REFERENCES

Alaback PB. 1996. Biodiversity Patterns in Relation to Climate: The Coastal Temperate Rainforests of North America. *High-Latitude Rainforests and Associated Ecosystems of the West Coast of the Americas Ecological Studies* 116: 105-133.

Agee JK. 1993. Fire Ecology of Pacific Northwest Forests. Washington D.C.: Island Press. 53 p.

C.D. Allen. 2009. Climate-induced forest dieback: an escalating global phenomenon? *Unasylva* 231/232 (60): 43-49

Allen CD, Macalady AK, Chenchouni H, Bachelet D, McDowell N, Vennetier M, Kitzberger T, Rigling A, Breshears DD, Hogg EH, Gonzalez P, Fensham R, Zhangui Z, Castro J, Demidova N, Lim JH, Allard G, Running SW, Semerci A, Cobb N. 2010. A global overview of drought and heat-induced tree mortality reveals emerging climate change risks for forests. *Forest Ecology and Management* 259 (4): 660-684.

Anderson JE, Plourde LC, Martin M, Braswell BH, Smith ML, Dubayah RO, Hofton MA, Blair JB. 2008. Integrating waveform lidar with hyperspectral imagery for inventory of a northern temperate forest. *Remote Sensing of Environment* 112 (4): 1856-1870.

Antonarakis AS, Richards KS, Brasington J. 2008. Object-based land cover classification using airborne LiDAR. *Remote Sensing of Environment* 112 (6): 2988-2998.

National Park Service, U.S. Department of the Interior. Auwaerter J, Sears JF. 2006. Historic Resource Study for Muir Woods National Monument: Land-Use History of Muir Woods. Olmstead Center for Landscape Preservation [last visited 2013 April 23]. Available from: <http://www.utm.utoronto.ca/asc/Handouts/CSE%20SBE%20Style%20Manual.pdf>.

Baatz M, Schäpe A. 2000. Multiresolution segmentation – an optimization approach for high quality multiscale image segmentation. In: *Angewandte Geographische Informationsverarbeitung XII. Beiträge zum AGIT-Symposium Salzburg, Karlsruhe, Herbert Wichmann Verlag: 12–23.*

Bayaga A. 2010. Multinomial Logistic Regression: Usage and Application in Risk Analysis. *Journal of Applied Quantitative Methods* 5 (2): 288-297.

- Bewick V, Cheek L, Ball J. 2004. Statistics Review 10: Further nonparametric methods. *Critical Care* 8 (3):196-199.
- Blaschke T. 2010. Object based image analysis for remote sensing. *Journal of Photogrammetry and Remote Sensing*. 65 (1): 2-16.
- Bork EW and Sue JG. 2009. Integrating LiDAR data and multispectral imagery for enhanced classification of rangeland vegetation: A meta analysis. *Remote Sensing of Environment* 111 (1): 11-24.
- Chapman JL and Reiss MJ. 2003. *Ecology: Principles and Applications*. New York: Cambridge University Press. 217-219 p.
- Chasmer L, Hopkinson C, Morrison H, Petrone R, Quinton W. 2011. Fusion of Airborne LiDAR and WorldView-2 MS Data for Classification of Depth to Permafrost within Canada's Sub-Arctic. *SilviLaser 2011*, Oct 16-20 [last visited 2013 April 12]. Available from: http://www.lo-cuscor.net/silvilaser2011/papers/072_Chasmer.pdf.
- Chust G, Galparsoro I, Borja A, Franco J, Uriarte A. 2008. Coastal and estuarine habitat mapping, using LiDAR height and intensity and multi-spectral imagery. *Estuarine, Coastal and Shelf Science* 78 (4): 633-643.
- Chan Y, Walmsley RP. 1997. Learning and Understanding the Kruskal-Wallis One-Way Analysis-of-Variance-by-Ranks Test for Differences Among Three or More Independent Groups. *Physical Therapy* 77: 1755-1761.
- Chen LC, Teo TA, Liu CL, 2006. The geometrical comparisons of RSM and RFM for FORMO-SAT-2 Satellite Images, *Photogrammetric Engineering & Remote Sensing* 72 (5): 573-579.
- Chen Y, Su W, Li J, Sun Z. 2008. Hierarchical object oriented classification using very high resolution imagery and LiDAR data over urban areas. *Advances in Space Research* 43 (7): 1101-1110.
- Cho MA, Skidmore AK, Sobhan I. 2009. Mapping beech (*Fagus sylvatica* L.) forest structure with airborne hyperspectral imagery. *International Journal of Applied Earth Observation and Geoinformation* 11 (3): 201-211.

Clark ML, Roberts DA, Clark DB. Hyperspectral discrimination of tropical rain forest tree species at leaf to crown scales. *Remote Sensing of Environment* 96 (3-4): 375-398.

Collin A, Planes S. 2012. Enhancing Coral Health Detection Using Spectral Diversity Indices from WorldView-2 Imagery and Machine Learners. *Remote Sensing* 4 (10): 3244-3264.

Congalton RG, Green K. 1999. Assessing the Accuracy of Remotely Sensed Data: Principles and Practices. New York: Lewis Publishers. 137 p.

Congalton RG, Green K. 2008. Assessing the Accuracy of Remotely Sensed Data: Principles and Practices, 2nd Ed. Boca Raton: CRC Press. 179 p.

Congalton RG. 1991. A Review of Assessing the Accuracy of Classifications of Remotely Sensed Data. *Remote Sensing of Environment* 37 (1): 35-46.

Dalponte M, Bruzzone L, Gianelle D. 2008. Fusion of Hyperspectral and LiDAR Remote Sensing Data for Classification of Complex Forest Areas. *IEEE Transactions on Geoscience and Remote Sensing* 46 (5): 1416-1427.

Darwish A, Leukert L, Reinhardt W. 2003. Image segmentation for the purpose of object-based classification. *Geoscience and Remote Sensing Symposium 3, IGARSS '03: 2039-2041*.

Davis W. 2000. Great Bear Rainforest. In: Rainforests: Ancient Realm of the Pacific Northwest. Toronto: Chelsea Green Publishing. 23-38 p.

DellaSala DA, Moola F, Alaback F, Spribille T, Wehrden HV, Nauman RS. Just what are Temperate and Boreal Rainforests. In: DellaSala DA, Moola F, Alaback F, Paquet PC, Schoen JW, Noss RF Temperate and Boreal Rainforests of the Pacific Coast of North America. New York: Island Press; 2011. p 1-41.

Dennison PE, Hallgan KQ, Roberts DA. 2004. A comparison of error metrics and constraints for multiple endmember spectral mixture analysis and spectral angle mapper. *Remote Sensing of Environment* 93 (3): 359-367.

DigitalGlobe [date unknown]. Orthorectifying DigitalGlobe Imagery in Erdas Imagine using the Rational Polynomial Coefficient (RPC) [last visited 2013 April 13]. Available

from:http://www.digitalglobe.com/downloads/partner_info/intergrapherdas/DigitalGlobe_RP_in_ERDAS_IMAGINE.pdf.

DigitalGlobe. 2010. White Paper: The Benefits of the 8 Spectral Bands of WorldView-2 [last visited 2013 March 14]. Available from: http://www.digitalglobe.com/downloads/World-View-2_8-Band_Applications_Whitepaper.pdf

Dymond JR, Shepherd JD, Qi J. 2001. A simple physical model of vegetation reflectance for standardising optical satellite imagery. *Remote Sensing of Environment* 77 (3): 230–239.

ENVI [date unknown]. ENVI Classic Tutorial: Using SMACC to Extract Endmembers [last visited 2013 April 23]. Available from: <http://www.exelisvis.com/portals/0/pdfs/envi/SMACC.pdf>.

Fraser CS, and Hanley HB. 2003. Bias compensation in rational functions for Ikonos satellite imagery. *Photogrammetric Engineering & Remote Sensing* 69 (1): 53–57.

Fraser CS, and Hanley HB. 2005. Bias-compensated RPCs for sensor orientation of high-resolution satellite imagery. *Photogrammetric Engineering & Remote Sensing* 71(8): 909–915.

Geerling GW, Garcia ML, Clevers JGPW, Ragas AMJ, Smits AJM. 2007. Classification of floodplain vegetation by data fusion of spectral (CASI) and LiDAR data. *International Journal of Remote Sensing* 28 (19): 4263–4284.

Giada S, De Groeve T. and Ehrlich D. 2003. Information extraction from very high resolution satellite imagery over Lukole refugee camp, Tanzania. *International Journal of Remote Sensing* 24 (22): 4251–4266.

Gu D and Gillespie A. 1988. Topographic normalization of Landsat TM images of forest based on subpixel sun-canopy-sensor geometry. *Remote Sensing of Environment* 64 (2): 166–175.

Hájek F. 2005. Object-oriented classification of remote sensing data for the identification of tree species composition. In: *Proceedings of Conference ForestSat 2005* 31 (5): 16–20.

Hayhoe K, Cayan D, Field CB, Frumhoff CB, Maurer EP, Moser SC, Schneider SH, Cahill KN, Cleland EE, Dale L, Drapel R, Hanemann M, Kalkstein LS, Lenihan J, Lunch

CK, Neilson Rp, Sheridan SC, and Verville JH. 2004. Emission pathways, climate change, and impacts on California. *Proceedings of the National Academy of Sciences of the United States of America*. 101 (34): 12422-12427.

Hosmer DW, Lemeshow S. 2000. Chapter 4. Model-Building Strategies and Methods for Logistic Regression. In: *Applied Logistic Regression*, 2nd Edition. New York: John Wiley & Sons. 91-142 p.

Hyde P, Dubayah R, Peterson B, Blair b, Hofton M, Hunsaker C, Knox R, Walker W. 2005. Mapping forest structure for wildlife habitat analysis using waveform lidar: Validation of montane ecosystems. *Remote Sensing of Environment* 96 (3/4): 427-437.

Jensen JR. 2005. Introductory Digital Image Processing: A Remote Sensing Perspective. Upper Saddle River: Prentice Hall. 495-515.

Jonckheere, A.R., 1954. A distribution-free k-sample test against ordered alternatives. *Biometrika* 41 (1/2), 133–145.

Jones TG, Coops NC, Sharma T. 2010. Assessing the utility of airborne hyperspectral and LiDAR data for species distribution mapping in the coastal Pacific Northwest, Canada. *Remote Sensing of Environment* 114 (12): 2841-2852.

Kamagata N, Hara K, Mori M, Akamatsu Y, LI Y, Hoshimo Y. 2008. Object-based classification of IKONOS data for vegetation mapping in Central Japan. In: Blaschke T, Lang S, Hay GJ.. Object-Based Image Analysis. *Lecture Notes in Geoinformation and Cartography*: 459-475.

Kane VR, Gillespie AR, MCGaughey R, Lutz, JA, Ceder K, Franklin JF. 2008. Interpretation and topographic compensation of conifer canopy self-shadowing. *Remote Sensing of Environment* 112 (10): 3820-3832.

Ke Y, Quackenbush LJ, Im J. 2010. Synergistic use of Quickbird multispectral imagery and LiDAR data for object-based forest species classification. *Remote Sensing of the Environment* 114 (6): 1141-1154.

Kempeneers P, Deronde B, Provoost S, Houthuys R. 2009. Synergy of Airborne Digital Camera and Lidar Data to Map Coastal Dune. *Journal of Coastal Research* 53 (Special Issue): 73-82.

Kimball LC and Kondolf M. Analysis of Channel Geomorphology and Habitat Forming Processes for Feasibility Assessment of Rip-Rap Removal, Muir Woods National Monument Mill Valley, California. Center for Environmental Design Research, Department of Landscape Architecture and Environmental Planning. The University of California, Berkeley [Internet]. 2002 [last visited 2013 April 16]. 20-65. Available from: http://ww.krisweb.com/biblio/southmarin_ucb_kimballetal_2002_riprap.pdf.

Kruskal WH, Wallis WA. 1952. Use of ranks in one-criterion variance analysis. *Journal of the American Statistical Association* 47 (260):583-621.

Liberte AS, Rango A, Herrick JE, Fredrickson EL, Burkett L. 2007. An object-based image analysis approach for determining fractional cover of senescent and green vegetation with digital plot photography. *Journal of Arid Environments* 69 (1) 1–14.

Lawford RG, Alaback P, Fuentes E. 1996. High-latitude rainforests and associated ecosystems of the West Coast of the Americas: climate, hydrology, ecology and conservation. New York: Springer, 228-23.

Majarau A, Palubinskas G, Reinartz P. 2011 Multi-sensor fusion for urban area classification. Joint Urban Remote Sensing Event - Munich, Germany. [last visited 2012 March 25]. Available from: http://elib.dlr.de/70025/1/006_Makarau_et_al.pdf.

McLaughlin RJ, Ellen SD, Blake MC, Jayko AS, Irwin WS, Aalto KS, Carver GA, Clarke SJ. 2000. Geology of the Cape Mendocino, Eureka, Garberville, and Southwestern part of the Hayfork 30 x 60 Minute Quadrangles and Adjacent Offshore Area, Northern California. Miscellaneous Field Studies MF-2336, Version 1.0. [last visited 2013 April 18] Available from <http://wrgis.wr.usgs.gov/map-mf/mf2336/ceghmf.pdf>

Mundt JT, Streutker DR, Glenn NF. 2006. Mapping Sagebrush Distribution Using Fusion of Hyperspectral and Lidar Classifications. *Photogrammetric Engineering & Remote Sensing* 72 (1): 47-54.

Myint SW, Gober P, Brazel A, Grossman-Clarke S, Weng Q. 2011. Per-Pixel vs. object-based classification of urban land cover extraction using high spatial resolution imagery. *Remote sensing of Environment* 115 (5): 1-17.

National Parks Conservation Association. 2011. State of the Parks, Muir Woods National Monument: A Resource Assessment [last visited 2013 April 17]. Available from:

http://www.npca.org/about-us/center-for-park-research/stateoftheparks/muir_woods/MuirWoods.pdf

National Park Service. 2008. Muir Woods: 100th Anniversary 2008 [last visited 2012 April 17]. Available from: <http://www.nps.gov/muwo/upload/unigrid-muwo.pdf>

Navulur K. 2007. *Multispectral Image Analysis Using the Object-Oriented Paradigm*. Boca Raton: CRC Press. 165 p.

Novack T, Esch T, Kux H and Stilla U. 2011. Machine Learning Comparison between WorldView-2 and QuickBird-2-Simulated Imagery Regarding Object-Based Urban Land Cover Classification. *Remote Sensing* 3 (10): 2263-2282.

Onojeghuo AO, Blackburn GA. 2011. Optimizing the use of hyperspectral and LiDAR data for mapping reedbed habitats. *Remote Sensing of Environment* 115 (8): 2025-2034.

Ozdemir I, Karnieli A. 2011. Predicting forest structural parameters using the image texture derived from WorldView-2 multispectral imagery in a dryland forest, Israel. *International Journal of Applied Earth Observation and Geoinformation* 13 (5): 701-710.

Petropoulos GP, Vadrevu KP, Xanthopoulos G, Karantounias G, Scholze M. 2010. A Comparison of Spectral Angle Mapper and Artificial Neural Network Classifiers Combined with Landsat TM Imagery Analysis for Obtaining Burnt Area Mapping. *Sensors* 10 (3): 1967-1985.

Plourde LC, Ollinger SV, Smith ML, Martin ME. 2007. Estimating Species Abundance in a Northern Temperate Forest Using Spectral Mixture Analysis. *Photogrammetric Engineering & Remote Sensing* 73 (7): 829-840.

Platt and Rapoza. 2008. An Evaluation of an Object-Oriented Paradigm for Land Use/Land Cover Classification. *The Professional Geographer* 60 (1) 87-100.

Pu R and Landry S. 2012. A comparative analysis of high spatial resolution IKONOS and Worldview-2 imagery for mapping urban tree species. *Remote Sensing of Environment* 124: 516-533.

Pu, R. L. 2004. Wavelet transform applied to EO-1 hyperspectral data for forest LAI and crown closure mapping. *Remote Sensing of Environment* 91 (2): 212-224.

Puttonen E, Suomalainen J, Hakala T, Raikkonen E, Kaartinen H, Kaasalainen S, Litkey P. 2010. Tree species classification from fused active hyperspectral reflectance and LiDAR measurements. *Forest Ecology and Management* 260 (10): 1843-1852.

Quackenbush LJ, Hopkins PF, and Kinn GJ. 2000. Developing Forestry Products from High Resolution Digital Aerial Imagery. *Photogrammetric Engineering Remote Sensing* 66 (11): 1337-1346.

Richter R, and Schlapfer D. 2012. Atmospheric / Topographic Correction for Satellite Imagery. Atcor-2/3 User Guide (8.2) [last visited 2013 March 12]. Available from http://www.rese.ch/pdf/atcor3_manual.pdf. 157 p.

Riggan ND and Weih RC. 2009. A Comparison of Pixel-based versus Object-based Land Use/Land Cover Classification Methodologies. *Journal of the Arkansas Academy of Science* 63: 145-152.

Robertson LD and King DJ. 2011. Comparison of pixel- and object-based classification in land cover change mapping. *International Journal of Remote Sensing* 32 (6): 1505-1529.

Rosso PH, Ustin SL, Hastings A. 2005. Mapping marshland vegetation of San Francisco Bay, California, using hyperspectral data. *International Journal of Remote Sensing* 26 (23): 5169-5191.

Salah M, Trinder J, Shaker A. 2009. Evaluation of the Self-Organizing Map Classifier for Building Detection from Lidar Data and Multispectral Aerial Images. *Journal of Spatial Science* 54 (2): 15-34.

Shackelford AK, Davis CH. 2003. A combined fuzzy pixel-based and object-based approach for classification of high-resolution multispectral data over urban areas. *IEEE Transactions on Geoscience and Remote Sensing* 41 (10): 2354-2363.

Shafri HZM, Suhaili A, Mansor S. 2007. The Performance of Maximum Likelihood, Spectral Angle Mapper, Neural Network and Decision Tree Classifiers in Hyperspectral Image Analysis. *Journal of Computer Science* 3 (6): 419-423.

Soenen S, Peddle DR, Coburn CA. 2005. SCS+C: A Modified Sun-Canopy-Sensor Topographic Correction in Forested Terrain. *Transactions on Geoscience and Remote Sensing* 43 (9): 2148-2159.

Stephens PR, Kimberly MO, Beets PN, Paul TSH, Searles N, Bell A, Brack C, Broadley J. 2012. Airborne scanning LiDAR in a double sampling forest carbon inventory. *Remote Sensing of Environment* 117: 348-357.

Strahler AH. 1980. The Use of Prior Probabilities in Maximum Likelihood Classification of Remotely Sensed Data. *Remote Sensing of Environment* 10 (2): 135-163.

Trimble. 2003. eCognition version 4.0.6 user guide, Definiens Imaging GmbH. Munich, Germany. 486 p.

Trimble. 2011. eCognition Developer 8.7: User Guide. Trimble Documentation, München, Germany.

Terpstra, T.J., 1952. The asymptotic normality and consistency of Kendall's test against trend, when ties are present in one ranking. *Proceedings of the Section of Sciences, Koninklijke Nederlandse Akademie van Wetenschappen* 55 (Series A), 327-333.

Tong X, Liu S, Weng Q. 2010. Bias-corrected rational polynomial coefficients for high accuracy geo-positioning of Quickbird stereo imagery. *Journal of Photogrammetry and Remote Sensing* 65 (2): 218-226.

Updike. T. 2010. Radiometric use of Worldview-2 Imagery. [last visited 2013 March 10]. Available from: http://www.digitalglobe.com/downloads/partner_info/intergrapherdas/DigitalGlobe_RP_in_ERDAS_IMAGINE.pdf.

Van Pelt R, Sillett SC, Nadkami NM. 2004. Quantifying and Visualizing Canopy Structure in Tall Forests: Methods and Case Study. In: Lowman MD and Rinker BH. *Forest Canopies*, 2nd Ed. San Diego: Elsevier: 49-65.

Voss M, Sugumaran R. 2008. Seasonal Effect on Tree Species Classification in an Urban Environment Using Hyperspectral Data, LiDAR, and an Object-Oriented Approach. *Sensors* 8 (5): 3020-3036.

Waring RH and Franklin. 1979. Evergreen Coniferous of the Pacific Northwest. *Science* 204 (No. 4400): 1380-1386.

Weishampel JF, Blair JB, Knox RG, Dubayah R, Clark DB. 2000. Volumetric lidar return patterns from an old-growth tropical rainforest canopy. *International Journal of Remote Sensing* 21 (2): 409-415.

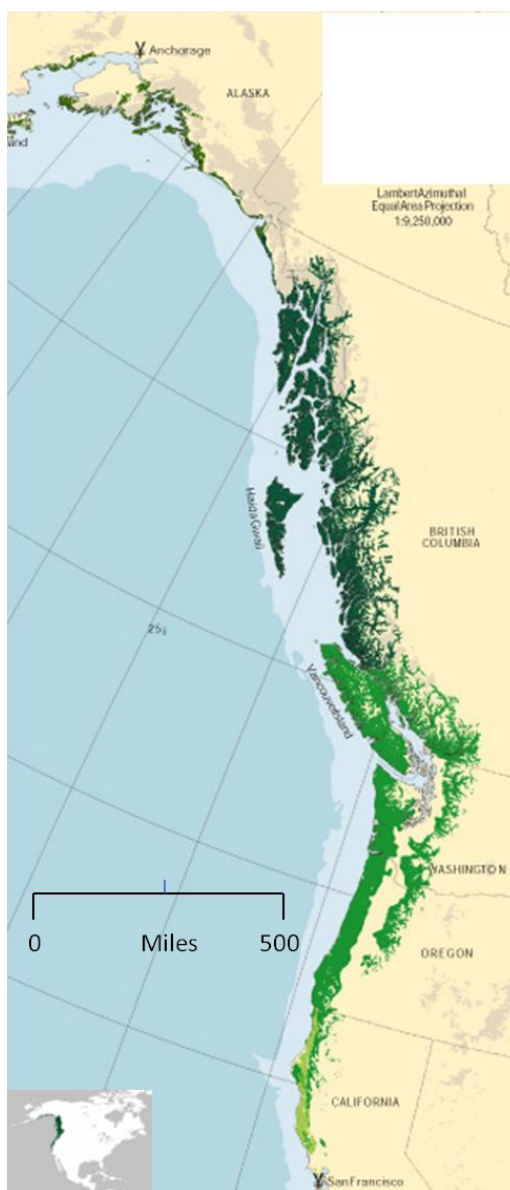
Xiao Q, Ustin SL, McPherson EG. Using AVIRIS data and multiple-masking techniques to map urban forest tree species. 2004. *International Journal of Remote Sensing* 25 (24): 5637-5654

Zhang C, and Qui F. 2012a. Mapping Individual Tree Species in an Urban Forest Using Airborne Lidar Data and Hyperspectral Imagery. *Photogrammetric Engineering & Remote Sensing* 78 (10): 1079-1087.

Zhang Z, De Wulf RR, Van Coillie FMB, Verbeke LPC, De Clercq EM, Ou Xiaokun. 2011. Influence of different topographic correction strategies on mountain vegetation classification accuracy in the Lancang Watershed, China. *Journal of Applied Remote Sensing* 5 (1): 124-126.

Zhang Z, Liu X, Wright W. 2012b. Object-based image analysis for forest species classification using Worldview-2 satellite imagery and airborne LiDAR data. In: International Symposium on Remote Sensing (ISRS 2012). 8th International Conference on Space, Aeronautical and Navigational Electronics (ICSANE 2012), 10-12 Oct 2012, Incheon, Korea.

APPENDIX 1: The Pacific Coast Temperate Rainforest



The Pacific Coast temperate rainforest biome is a region with a broad range of physiological landscape types that influence many varied ecological processes (Lawford *et al.* 1996). The old-growth temperate rainforests thrive in the coastal mountain ranges from the San Francisco Bay Area to Southern Alaska. The montane landscape ensnares the maritime air masses full of moisture arising from the Pacific Ocean. As this moisture condenses into rain it creates lush rainforests with the largest tree in the world -- the coastal redwood (DellaSalla *et al.* 2011). According to Alaback (1996), this biome has the following characteristics:

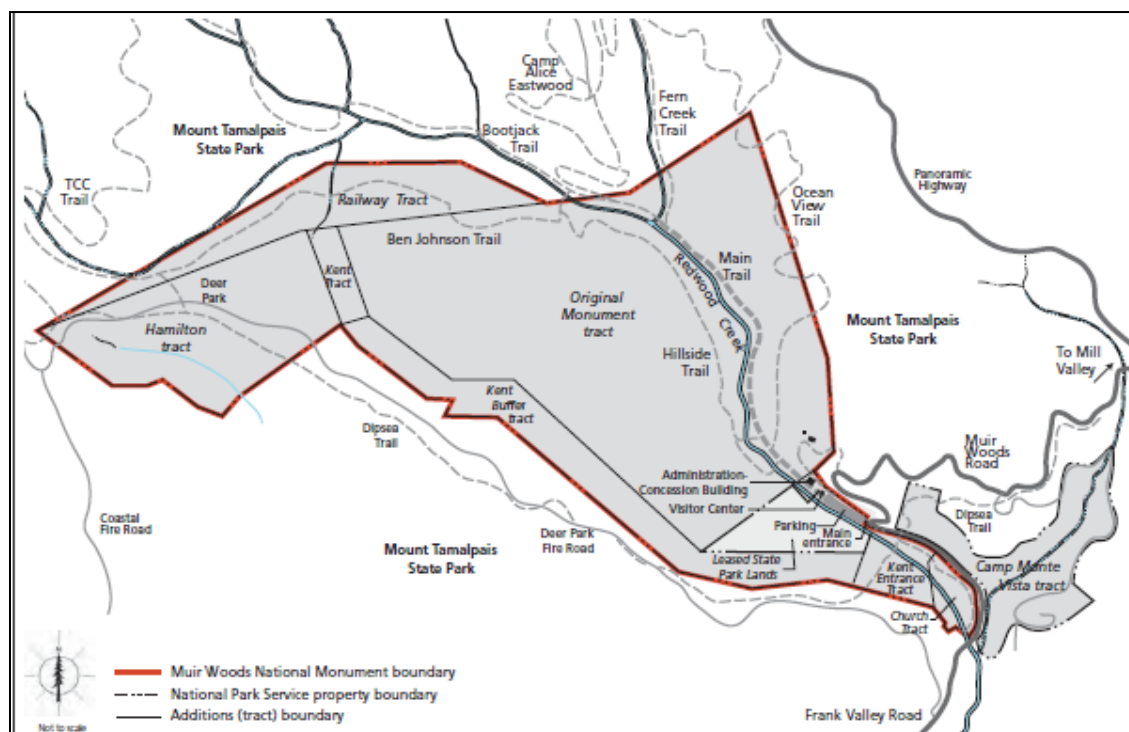
- Gradient from 38⁰N to 61⁰N
- A maritime and coastal montane climates with 1400mm rainfall or greater
- Cool temperatures throughout the year (4°C to 20°C)

Legend

Pacific Coast Temperate Rainforest Type:	
	Subpolar Temperate Rainforest (Alaska)
	Perhumid Temperate Rainforest
	Seasonal Temperate Rainforest
	Coastal Redwood Warm Temperate Rainforest
	Snow/Ice Barren

Image Source: Ecotone (www.inforain.org/)

APPENDIX 2: Map of Muir Woods



Source: Auwaerter and Sears 2006.

APPENDIX 3: Calibration Coefficients of WV2 Image

Sensor calibration is a procedure to pertaining to spectral properties, where channel center positions or radiometric properties, (i.e., the offset (C_0) and slope (C_1) coefficients, relating the digital number to the at-sensor radiance) may have changed. For multispectral imagery, spectral calibration problems are difficult to detect (Richter and Schlapfer 2012). This calibration fixes possible problems in the spectral response curve of each band. Only C_1 is corrected per WV2 image, and each image will have different C_1 coefficients . The calibration file is located in the metadata file of the raw image file. C_1 was corrected and calculated as follows (taken from Richter and Schlapfer 2012):

$$C_1 = 0.1 * \text{radiometric gain factor [k]} / \text{effective Bandwidth} \quad [3]$$

Calibrated Gain Settings for WV2 Image over Redwood Canyon

Band	C_0	C_1 (mW/cm ² sr micron]
1	0.0	0.0196525
2	0.0	0.0328467
3	0.0	0.0216539
4	0.0	0.0155877
5	0.0	0.0192268
6	0.0	0.1320136
7	0.0	0.1237998
8	0.0	0.0090786

APPENDIX 4: Tools Used for Collecting Training Samples

The stratified random samples were collected in the summer of 2012. Tools and references used for the sampling included the following:

- Bushnell Falcon 10x50 Wide Angle Binoculars
- *Tree Finder: A Manual for the Identification of Trees by their Leaves*, by May Watts (1998)
- *Pacific Coast Tree Finder: A Pocket manual for identifying Pacific Coast trees*, 2nd Ed. by Tom Watts (2004)
- *The Laws Field Guide to the Sierra Nevada*, by John Laws (2007).
- 2 JUNO GPS Receivers by the manufacturer Trimble, using the pre-installed Terrasync software for GPS data collection and maintenance.
- Muir Woods and Mt. Tamalpais State Park trail maps
- A notebook for data entry and to sketch maps to aid in visualization.